HHS Public Access

Author manuscript

Curr Biol. Author manuscript; available in PMC 2024 February 27.

Published in final edited form as:

Curr Biol. 2023 February 27; 33(4): 607–621.e7. doi:10.1016/j.cub.2022.12.041.

A BORC-dependent molecular pathway for vesiculation of cell corpse phagolysosomes

Gholamreza Fazeli[1,2,*], **Roni Levin-Konigsberg**[3], **Michael C. Bassik**[3], **Christian Stigloher**[2], **Ann M. Wehman**[4,*]

[1]Rudolf Virchow Center for Integrative and Translational Bioimaging, University of Würzburg, 97080 Wurzburg, Germany

[2]Imaging Core Facility, Biocenter, University of Würzburg, 97074 Würzburg, Germany

[3]Department of Genetics, Stanford University School of Medicine, Stanford, CA 94305, USA.

[4]Department of Biological Sciences, University of Denver, Denver, CO 80208, USA

Summary

Phagocytic clearance is important to provide cells with metabolites and regulate immune responses, but little is known about how phagolysosomes finally resolve their phagocytic cargo of cell corpses, cell debris, and pathogens. While studying the phagocytic clearance of non-apoptotic polar bodies in *C. elegans*, we previously discovered that phagolysosomes tubulate into small vesicles to facilitate corpse clearance within 1.5 hours. Here, we show that phagolysosome vesiculation depends on amino acid export by the solute transporter SLC-36.1 and the activation of TORC1. We demonstrate that downstream of TORC1, BLOC-1-related complex (BORC) is de-repressed by Ragulator through the BORC subunit BLOS-7. In addition, the BORC subunit SAM-4 is needed continuously to recruit the small GTPase ARL-8 to the phagolysosome for tubulation. We find that disrupting the regulated GTP-GDP cycle of ARL-8 reduces tubulation by kinesin-1, delays corpse clearance, and mislocalizes ARL-8 away from lysosomes. We also demonstrate that mammalian phagocytes use BORC to promote phagolysosomal degradation, confirming the conserved importance of TOR and BORC. Finally, we show that HOPS is required after tubulation for the rapid degradation of cargo in small phagolysosomal vesicles, suggesting that additional rounds of lysosome fusion occur. Thus, by observing single phagolysosomes over time, we identified the molecular pathway regulating phagolysosome vesiculation that promotes efficient resolution of phagocytosed cargos.

[*]**Corresponding authors:** Gholamreza Fazeli (gholamreza.fazeli@uni-wuerzburg.de), Ann M Wehman (ann.wehman@du.edu).

Author Contributions

G.F. designed, performed, analyzed, and supervised most worm experiments and wrote the manuscript together with R.L.K. and A.M.W. R.L.K. designed, performed, and analyzed mammalian CRISPR experiments. M.C.B. and C.S. supervised experiments. A.M.W. designed and supervised experiments, performed light sheet microscopy, and analyzed data.

Declaration of Interests

The authors declare no competing commercial interests related to this work.

Graphical Abstract

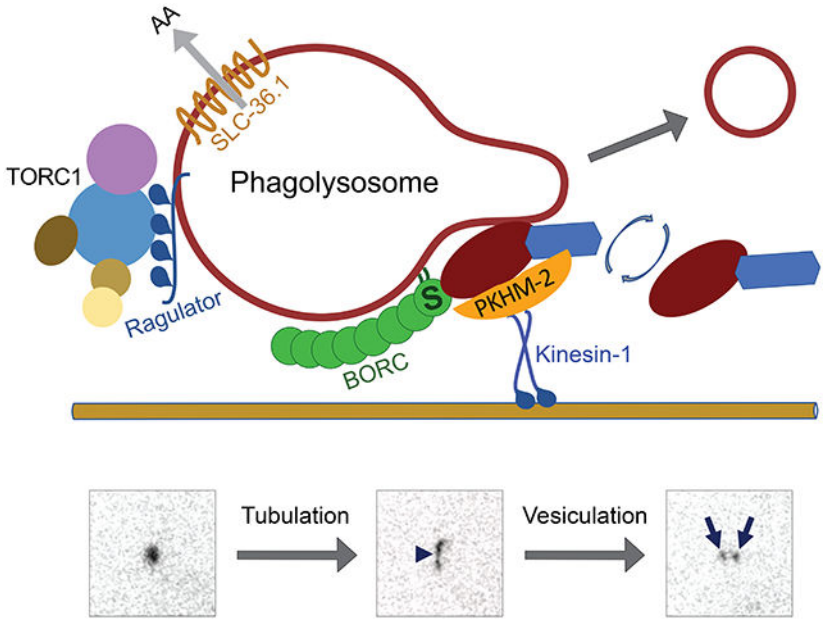

Cells use phagocytosis to engulf and degrade dying cells in phagolysosomes, but cell corpses are often larger than lysosomes. Fazeli *et al.* identify the molecular pathways used by *C. elegans* embryos and mammalian macrophages to tubulate large phagolysosomes into smaller vesicles for rapid lysosomal degradation and phagolysosome resolution.

Keywords

Phagolysosome resolution; cell corpse clearance; phagosome maturation; small GTPase; polar body

Introduction

Phagocytosis is an essential part of the innate immune response to pathogens as well as a key element for tissue homeostasis through the clearance of dying cells and debris. Billions of cell corpses are removed from the human body every day, which is important to avoid auto-immune responses[1]. Many cell types, including undifferentiated cells, use phagocytosis to engulf and eventually degrade phagocytosed cargo[1,2]. The mechanisms of phagocytic engulfment and phagosome-lysosome fusion are well studied, but there is little known about how phagolysosomal dynamics influence cargo degradation, which is important for nutrient acquisition and to modulate the immune response[3]. The final stage where a phagolysosome resolves, degrading all cargo and recycling its lipid membrane to endolysosomal pathways, is a mystery due to challenges observing late stages in phagolysosome resolution. In most experimental systems, it is difficult to predict when a phagocytic event will occur and unambiguously track an individual phagolysosome for long periods. Furthermore, the study of non-degradable phagocytic cargos, such as inorganic beads, has precluded analysis of the ultimate stages of phagocytic clearance.

We previously showed that a cell corpse, the second polar body, is phagocytosed by large blastomeres within a 15-minute window in early *C. elegans* embryos[4]. We found that cargo degradation occurs rapidly, ~90 minutes after phagosome-lysosome fusion, allowing us to image phagolysosomal dynamics during resolution *in vivo*. We discovered that phagolysosomes tubulate to form small vesicles that rapidly degrade corpse proteins (Figure 1A-B, Video S1)[4]. The fragmentation of large phagosomes into smaller cargo-containing vesicles has been observed with diverse cargo, including germ cell lobes, neuronal exophers, apoptotic and entotic cells[5-7]. When phagolysosomal vesiculation was inhibited, protein degradation was delayed by over an hour[4], revealing that vesiculation promotes cargo degradation. This process is distinct from lysosome reformation after autophagy or phagocytosis[8,9], as the phagolysosomal vesicles contain undegraded cargo[4,5,10].

We previously found that the mTOR ortholog LET-363 was required for vesiculation of the polar body phagolysosome[4], consistent with observations in cultured mouse macrophages[5]. Decreased vesiculation of the phagolysosome delayed degradation of its protein content[4], revealing the importance of subdividing large phagolysosomes to ensure efficient degradation. mTOR is found in two lysosomal complexes, mTORC1 and mTORC2, which are activated by different signals and activate distinct downstream signaling targets[11]. However, it was unknown which proteins upstream or downstream of mTOR were involved in phagolysosome vesiculation.

We also discovered that the small ARF-like GTPase ARL-8 is required for phagolysosome tubulation and cargo degradation[4]. ARL-8 cycles between a GDP-bound and GTP-bound state[12], and GTP-bound ARL-8 can interact with kinesin motor proteins to mediate axonal transport of synaptic vesicles[13,14]. Intriguingly, mammalian ARL8 localizes to lysosomes and promotes their anterograde transport by kinesins through an adapter protein PLEKHM2[15]. Therefore, we hypothesized that ARL-8 links the phagolysosome membrane to motor proteins on microtubules to extend tubules and release vesicles[4], however it was unclear whether GTP-bound ARL-8 was sufficient to drive phagolysosomal tubulation or whether TOR and ARL-8 were part of the same pathway regulating tubulation.

During organelle transport, ARL8 has been connected to the BLOC-1-related complex BORC[16-19]. BORC is a multi-subunit complex that localizes on the lysosomal membrane via the myristoyl group of its mammalian subunit Myrlysin[16]. The Myrlysin ortholog SAM-4 binds to nucleotide free ARL-8, recruiting ARL-8 to the lysosome, and is thought to act as a guanine nucleotide exchange factor (GEF)[18]. ARL8 recruitment to lysosomes also depends on the BORC subunit Lyspersin[20,21], which interacts with LAMTOR/Ragulator, a lysosomal complex that recruits and activates mTOR[20,21,22]. BORC plays a role in lysosome tubulation[16], but it was unknown whether BORC could regulate phagolysosome vesiculation.

Here, we report that phagolysosome tubulation occurs after amino acid release by solute carriers and the activation of TORC1 to relieve an interaction between Ragulator and BORC. BORC then activates ARL-8 for tubulation of the phagolysosome by kinesin-1. We also discovered that BORC proteins are required to resolve phagolysosomes in mammalian cells. Both GDP- and GTP-locked mutants of *arl-8* show reduced tubulation of the phagolysosome

and disrupt ARL-8 localization, revealing that ARL-8 needs to cycle to promote tubulation on phagolysosomes. Finally, the HOPS tethering complex, an ARL-8 effector that promotes lysosome fusion[12], is required to rapidly degrade cargo in the small phagolysosomal vesicles released by phagolysosome tubulation, suggesting that the vesicles undergo additional lysosome fusion events. Thus, using an *in vivo* model to observe resolution of a single phagolysosome, we have identified a conserved molecular pathway regulating tubulation and vesiculation to promote degradation of phagolysosome cargos.

Results

Phagolysosome vesiculation requires amino acid release and TORC1 activation

To determine which TOR complex is involved in phagolysosome tubulation in *C. elegans*, we depleted TORC1 and TORC2 subunits that define the substrate specificity of each complex, specifically the Raptor ortholog DAF-15 for TORC1 and the Rictor ortholog RICT-1 for TORC2 and examined polar body phagolysosome dynamics. Similar to the two-fold decrease in phagolysosome fission events we saw after depleting TOR[4], treatment with *daf-15* RNAi resulted in a two-fold decrease in fission events (Figure 1C-D). Phagolysosomes also remained large and the degradation of polar body protein cargo was delayed over an hour after depleting DAF-15 (Figure 1C, F), similar to TOR[4]. In contrast, *rict-1* RNAi did not significantly affect vesiculation (Figure 1D) but did lead to a half hour delay in phagolysosomal degradation (Figure 1F). These findings suggest that only TORC1 is required for phagolysosome vesiculation (Table S1), but that both TORC1 and TORC2 play important roles in phagolysosomal degradation.

To confirm that the TORC1 pathway is involved in vesiculation, we next disrupted predicted upstream regulators of TORC1. TORC1 is activated by amino acid release by solute carriers, including SLC-36.1 orthologs[23,24], and inhibited by AMP Kinase, which can directly phosphorylate Raptor[25,26]. Knockdown of *slc-36.1* decreased the number of fission events by half and delayed degradation of the phagolysosome over 40 minutes (Figure 1C-D, F), consistent with amino acid release promoting vesiculation. In contrast, deleting the AMPK catalytic subunit AAK-2 resulted in a 60% increase in vesiculation in *aak-2(ok524)* mutants (Figure 1D-E), consistent with AAK-2 negatively regulating phagolysosome vesiculation. Increased vesiculation did not lead to faster clearance of polar body contents (Figure 1F), raising the possibility that other lysosomal factors are limiting for protein degradation. To test whether lysosome function was altered in *aak-2* mutants, we analyzed the time it took for protein in phagolysosomal vesicles to be degraded. There was no significant change in disappearance timing (Figure S1A), demonstrating that lysosomal degradation is intact in *aak-2* mutants. However, we did observe a significant 4-fold increase in the number of vesicles that disappeared within one frame of their release (Figure S1B), raising the possibility that the increased vesiculation events in AMPK mutants created more small vesicles rather than significantly reducing the size of the main phagolysosome. Thus, TORC1 activators and inhibitors also modulate vesiculation and degradation of phagolysosomal cargos.

BORC is required for phagolysosome tubulation and resolution

As the lysosome-resident BORC complex is required during organelle transport and tubulation[16-19], we asked whether BORC subunits promote phagolysosome vesiculation, starting with the Myrlysin ortholog SAM-4[18]. In *sam-4(tm3828)* mutants, phagolysosomes remained large (Figure 2A), we observed a five-fold decrease in phagolysosome vesiculation (Figure 2B), and degradation of the phagolysosome contents was delayed over an hour (Figure 2C). Loss-of-function mutants for BORC subunits *BORCS1/blos-1(ok3707)*, *BORCS2/blos-2(js1351)*, and *Lyspersin/blos-7(wy1159)* also reduced vesiculation by five-fold and delayed degradation over an hour (Figure 2A-C, Video S2, Table S1). These results demonstrate that the major subunits of BORC are required for phagolysosome vesiculation and the timely degradation of a cell corpse.

BORC also contains variable subunits that have disparate roles in organelle transport: KXD1 and Diaskedin are specifically required for lysosome transport[16], while the MEF2BNB ortholog BLOS-9 is specifically required for synaptic vesicle transport[18]. Phagolysosome tubulation and degradation occurred normally in mutants for the Diaskedin ortholog *blos-8(js1354)* and for *blos-9(js1352)* (Figure 2A-C), while degradation of the phagolysosome was delayed almost an hour in *kxd-1(js1356)* mutants (Figure 2C). These findings suggest that the variable BORC subunits have separable functions in synaptic vesicle transport, lysosome transport, or phagolysosomal degradation (Table S1). Interestingly, *kxd-1(js1356)* mutants showed a bimodal vesiculation phenotype, with half normal and half disrupted (Figure 2B), leaving open the possibility that variable BORC subunits play redundant roles in phagolysosomal vesiculation. To test this, we generated *blos-8(js1354); kxd-1(js1356)* double mutant embryos and discovered that phagolysosome vesiculation was reduced five-fold and cargo degradation was delayed over an hour, similar to the major BORC subunits (Figure 2A-C). These data indicate that the variable BORC subunits have distinct, but partially overlapping functions and implicate the subunits involved in lysosome transport in phagolysosome degradation.

BORC subunits BLOS-1 and BLOS-2 also act in a related complex BLOC-1, which is involved in the biogenesis of lysosome-related organelles[27]. Therefore, we tested whether the BLOC-1-specific subunit Pallidin/GLO-2 has a role in phagolysosome tubulation. Vesiculation and degradation occurred normally in strong loss-of-function *glo-2(zu455)* mutants (Figure 2A-C, Table S1), suggesting that BLOS-1 and BLOS-2 act as part of the BORC complex in phagolysosome resolution.

Phagolysosome vesiculation via BORC is conserved in mammals

We next asked whether BORC is needed to vesiculate phagolysosomes in mammals. We fed murine macrophage J774 cells with opsonized sheep red blood cells (SRBC). 6 hours later, engulfed SRBC were fragmented throughout the cytoplasm of engulfing cells (Figure 2F), confirming previous work[28]. We mutated BORC subunits Lyspersin and Myrlysin using CRISPR/Cas9 (Figure S2) and found that SRBC fragmentation (stage III) was reduced in mutant clones, with more SRBCs remaining intact (stage I) or forming only a few fragments (stage II) (Figure 2G-I). These data suggest that the role of BORC in phagolysosome vesiculation is conserved from nematodes to mammals.

BORC and TORC1 act on the same pathway for phagolysosome vesiculation

We next tested whether TORC1 and BORC act on the same or parallel pathways regulating phagolysosome vesiculation. The BORC subunit Lyspersin binds to LAMTOR2[20,21], a Ragulator subunit that acts as a GEF for Rag GTPases to recruit mTORC1 to lysosomes[29,30]. LAMTOR2 binding to Lyspersin inhibits BORC to prevent ARL8-mediated lysosome transport[20,21]. Therefore, we asked whether disrupting LMTR-2 would activate BORC and bypass the requirement for TORC1 in phagolysosome vesiculation. In *lmtr-2*(*tm2367*) deletion mutants, phagolysosome vesiculation was reduced over five-fold and degradation was delayed by over an hour (Figure 1D, F, Table S1). Given that Ragulator is required for mTORC1 recruitment[29,30], the similar phenotype of *lmtr-2*(*tm2367*) mutants to TORC1-deficient embryos could be due to TORC1 not being recruited to the phagolysosome. Thus, Ragulator is likely to have multiple roles regulating both BORC and TORC1 during phagolysosome vesiculation.

To separate the roles of Ragulator in TORC1 recruitment and BORC regulation, we generated a *blos-7(L30A)* mutant analogous to mammalian Lyspersin L221A (Figure S3A), which is deficient in binding to LAMTOR2[21]. We observed no changes in phagolysosome vesiculation in *blos-7(L30A)* mutants compared to controls (Figure 2D), indicating that relieving LMTR-2 inhibition was not sufficient for premature or increased phagolysosome vesiculation by BORC. This further supports that the *lmtr-2* deletion phenotype is likely caused by failing to recruit TORC1.

To determine whether TORC1 acts upstream of BORC, we tested whether TOR knockdown was able to disrupt phagolysosome vesiculation in *blos-7(L30A)* mutants. Knocking down *let-363/TOR* in *blos-7(L30A)* mutants resulted in a normal number of fission events (Figure 2D), suggesting that TORC1 activity relieves BORC inhibition through LMTR-2. Treating *blos-7(L30A)* mutants with *let-363* RNAi still resulted in sterility and embryonic lethality, confirming the efficacy of the knockdown. These data suggest that TORC1 regulates phagolysosome resolution in the same pathway as the Ragulator-BORC interaction.

To confirm that BORC acts downstream of the TORC1 pathway in phagolysosome resolution, we asked whether deleting *sam-4* could suppress TORC1 activation caused by disrupting AMPK. The polar body phagolysosome in *sam-4(tm3828); aak-2(ok524)* double mutants showed a five-fold reduction in vesiculation (Figure 2E), similar to *sam-4(tm3828)* mutants (Figure 2B), which was significantly different from controls or *aak-2* single mutants (Figure 1D). These data place BORC downstream of TORC1 activation in the same pathway regulating phagolysosome vesiculation.

To test whether amino acid transport acts upstream of TORC1 activation or Ragulator inhibition in phagolysosome vesiculation, we depleted SLC-36.1 in activated TORC1 mutants and disinhibited BORC mutants. Knocking down SLC-36.1 in *aak-2* or *blos-7(L30A)* mutants decreased the number of fission events by half or more (Figure 2D-E), similar to *slc-36.1* knockdown in a control strain (Figure 1D). These results suggest that the export of neutral amino acids from the phagolysosome can regulate tubulation independent of TORC1 activation or BORC inhibition.

To determine whether amino acid transport acts via a parallel pathway to BORC in phagolysosome vesiculation, we tested whether we can further reduce fission events in *Lyspersin/blos-7* deletion mutants by depleting SLC-36.1. We did not observe a decrease in the number of fission events in *blos-7(wy1159)* mutants treated with SLC-36.1 RNAi (Figure 2E), suggesting that amino acid transport by SLC-36.1 and BORC may converge on the same pathway regulating phagolysosome tubulation.

The ARL-8 GTPase must cycle between GDP- and GTP-bound states for phagolysosome tubulation

We next asked whether ARL-8 acts downstream of TORC1 in phagolysosome tubulation using a partial loss-of-function *arl-8(wy271)* mutant (Figure 3A)[13]. Consistent with *arl-8* knockdown[4], phagolysosome vesiculation was reduced five-fold and degradation was delayed over an hour in *arl-8(wy271)* deletion mutants (Figure 3B-D). Activating TORC1 in *arl-8(wy271); aak-2(ok524)* double mutants showed similarly decreased phagolysosome fission events and delayed degradation (Figure 3B-D), confirming that both ARL-8 and BORC act downstream of TORC1 activation in phagolysosome resolution.

As BORC recruits nucleotide-free ARL-8 and promotes GTP exchange for ARL-8[18], we asked how the bound nucleotide dictates the activity of ARL-8 during phagolysosome tubulation. We generated point mutations in endogenous ARL-8 predicted to lock the GTPase in either a GDP- or GTP-bound state[31]. GDP-bound *arl-8(T34N)* mutants reduced vesiculation five-fold and delayed degradation over an hour (Figure 3B-D), consistent with predictions ARL-8(T34N) is inactive[31]. GTP-locked *arl-8(Q75L)* mutants decreased vesiculation two-fold and delayed phagolysosome degradation over an hour (Figure 3B-D), in contrast to findings that ARL-8(Q75L) can rescue synaptic vesicle trafficking defects[13] or embryonic lethality of the strong loss-of-function *arl-8(tm2504)* deletion allele[32]. We next examined mutations in the GTPase G4 motif predicted to allow nucleotide exchange independent of a GEF[33] and able to rescue synaptic vesicle trafficking defects[18]. We observed a five-fold reduction in phagolysosome vesiculation and an hour delay in cargo degradation with *arl-8(D133A)* or *arl-8(D133N)* mutants (Figure 3B-D). These data indicate that both GDP- and GTP-locked as well as unlocked alleles disrupt phagolysosome tubulation and suggest that ARL-8 needs to cycle between GDP- and GTP-bound in a controlled fashion to regulate phagolysosome vesiculation and resolution.

ARL-8 localization depends on its nucleotide state

To understand how ARL-8 localization is affected by its nucleotide state, we tagged endogenous ARL-8 with mCitrine (Figure 3A). The ARL-8::mCit knock-in did not alter vesiculation events (Figure 3C), suggesting that ARL-8::mCit promoted phagolysosome vesiculation normally. However, degradation of polar body phagolysosome content was delayed by half an hour (Figure 3B, D), suggesting that the fluorescent tag may have a minor effect on another aspect of ARL-8's function in phagolysosomal cargo degradation. ARL-8::mCit localized to punctate structures in early embryos (Figure 4B-C), which we confirmed were 50 ± 6% lysosomal by colocalization with an mScarlet-I-tagged lysosome-resident BORC subunit SAM-4::mSc (Figure 4M, S4A-B). We also confirmed that SAM-4::mSc colocalized with the endogenously-tagged lysosomal marker

Cystinosin/CTNS-1::mCit (Figure S4C). 10 ± 1% of ARL-8::mCit also colocalized with the early endosomal small GTPase mCh::RAB-5 (Figure 4N), consistent with overexpression studies showing that ARL-8::GFP localized to lysosomes but was also observed on other structures[34]. ARL-8::mCit-positive puncta started appearing around the polar body phagosome shortly after engulfment and ARL-8 appeared as a ring around the phagolysosome 6 ± 2 minutes after engulfment (n=8, Figure 4A), similar to the timing of LMP-1-positive lysosome recruitment[4], which suggests that ARL-8 is recruited to the phagosome at lysosome fusion.

We next generated point mutations altering the nucleotide cycle in the *arl-8*::mCit knock-in strain and examined their localization. GDP-bound ARL-8(T34N)::mCit appeared dispersed and did not localize to the polar body phagolysosome (Figure 4B, D, S5C), consistent with GTP binding promoting insertion of an amphipathic helix into lipid bilayers for membrane localization[35]. GTP-locked ARL-8(Q75L)::mCit localized on enlarged tubulovesicular structures, the plasma membrane and the ER (Figure 4B, E, S5A), but was not observed on discrete puncta indicative of endolysosomes. ARL-8(Q75L)::mCit localized to the polar body plasma membrane before phagocytosis (Figure S5G), in addition to the phagosome membrane immediately after engulfment (Figure S5D), consistent with its localization to plasma membranes. In contrast, unlocked ARL-8(D133N)::mCit and ARL-8(D133A)::mCit localized to large tubulovesicular structures and other unidentified structures that appeared distinct from cytosolic dispersion (Figure 4B, F-G), but not the plasma membrane, ER, or polar body phagolysosome (Figure 4F-G, S5B, E-F). The large tubulovesicular structures in *arl-8(D133N)* mutants colocalized with mCh::RAB-5 (Figure 4O), revealing that interfering with the regulated GDP/GTP cycle traps ARL-8 on early endosomes and alters endosomal morphology. Thus, a regulated cycle between the GDP- and GTP-bound states is required for ARL-8 lysosome localization and phagolysosome tubulation.

BORC but not TORC1 is required for ARL-8 localization to lysosomes and the phagolysosome

As Myrlysin is required for ARL8 localization to lysosomes in HeLa cells[16], we asked whether SAM-4 or other BORC subunits are required for ARL-8 localization to the polar body phagolysosome. ARL-8::mCit was not observed on the polar body phagolysosome in *sam- (tm3828)* mutants (Figure 5A). Instead, ARL-8::mCit associated with large tubulovesicular networks in *sam-4(tm3828)* mutants (Figure 4I), which we confirmed to be early endosomes by colocalization with mCh::RAB-5 (Figure 5B) and excluded as lysosomes by LMP-1 staining (Figure 5C). ARL-8::mCit similarly associated with enlarged tubulovesicular networks in *blos-1(ok3707)* and *blos-7(wy1159)* mutants (Figure 4J-K). Thus, BORC is required for both the lysosomal and phagolysosomal localization of ARL-8, suggesting that the phagolysosome resolution defects in BORC mutants are likely caused by altering ARL-8 localization.

Next, we asked whether proteins upstream of BORC also alter ARL-8 localization. We saw no gross changes to ARL-8::mCit localization after disrupting phagolysosomal amino acid export with *slc-36.1* RNAi (Figure S4E), disrupting TORC1 with *TOR/let-363* or *Raptor/daf-15* RNAi (Figure 4H, S4F), over-activating TORC1 in *AMPK/aak-2(ok524)*

deletion mutants (Figure S4G), or disrupting TORC1 recruitment and BORC inhibition in *lmtr-2(tm2367)* mutants (Figure S4H). Similarly, ARL-8::mCit remained punctate (Figure 4L) and localized to the polar body phagolysosome in disinhibited *blos-7(L30A)* mutants (Figure S3B). We further confirmed that *TOR/let-363* RNAi did not significantly alter ARL-8::mCit colocalization with SAM-4 (Figure S4A-B, D). These data indicate that BORC regulates ARL-8 localization independent of TORC1 activity and LAMTOR inhibition, leaving the molecular impact of ARL-8 regulation by TORC1 and Ragulator unclear.

As BORC deletion leads to chronic disruption of ARL-8 localization, which could affect lysosomes, we used a degron approach to determine the effect of acute loss of SAM-4 on ARL-8 localization and phagolysosomal degradation. We tagged endogenous SAM-4 with mScarlet-I and a ZF1 degron to induce ZIF-1-mediated degradation starting in anterior cells at the 4-cell stage (Figure 5D-E)[36], which is around the time of the polar body phagocytosis[4]. Prior to degradation, ARL-8::mCit localized on discrete puncta (half together with SAM-4::mSc::ZF1) (Figure 5D). Within 20 minutes of SAM-4::mSc::ZF1 degradation, ARL-8::mCit dispersed (Figure 5E). ARL-8::mCit was also not observed on the polar body phagolysosome after SAM-4::mSc::ZF1 degradation (Figure S5H). These data suggest that SAM-4 is needed to maintain ARL-8 localization to lysosomal and phagolysosomal membranes.

To confirm that lysosomes are intact after SAM-4 degradation, we examined an Cystinosin/CTNS-1::mCit in SAM-4::mSc::ZF1 mutants. The punctate pattern of CTNS-1::mCit did not change after the onset of degradation (Figure S6), indicating that lysosome morphology was not altered by SAM-4 depletion. Thus, degradation of SAM-4 leads to the mislocalization of ARL-8 from lysosomes, not the loss of lysosomes.

Interestingly, we did not observe ARL-8::mCit on enlarged endosomes before the 24-cell stage, almost an hour after SAM-4::mSc::ZF1 degradation began. After the 24-cell stage, 27% of the SAM-4::mSc::ZF1 embryos showed ARL-8::mCit on enlarged endosomes in addition to diffuse signal (n=30), in contrast to 75% of *sam-4* deletion mutants (Figure 4B, n=20). These observations indicate that endosome enlargement and/or the mislocalization of ARL-8 to enlarged endosomes needs at least an hour or lower SAM-4 levels than we achieve with ZF1 degron tagging.

We then asked how phagolysosomal vesiculation and resolution are affected by acute loss of SAM-4 and mislocalization of ARL-8. SAM-4::mSc::ZF1 embryos showed a two-fold decrease in phagolysosome fission events and delayed degradation by half an hour (Figure 5F-H). These data indicate that SAM-4 constantly recruits ARL-8 to lysosomal and phagolysosomal membranes to tubulate and degrade phagolysosome cargo.

Kinesin-1 is required for phagolysosome tubulation

We next asked which proteins drive phagolysosome tubulation downstream of ARL-8. Mammalian ARL8 binds to SKIP/PLEKHM2 for anterograde transport by kinesin-1[15], as well as binding kinesin-3 directly[14]. We screened kinesin-1 using the KIF5 ortholog UNC-116 and kinesin-3 using the KIF1 ortholog UNC-104. As strong loss-

of-function *unc-116* mutants disrupt the birth of the polar body[37], we generated an UNC-116::mCit::ZF1 strain, which degrades UNC-116 after the polar body is engulfed (Figure 6A). Phagolysosome vesiculation showed a 2-fold decrease after UNC-116::mCit::ZF1 degradation and the resolution of phagolysosomal cargo was delayed by 30 minutes (Figure 6B-D). In contrast, neither the number of fission events nor the timing of degradation was affected in the *unc-104(e1265)* reference allele (Figure 6B-C). These data demonstrate that kinesin-1, not kinesin-3 (Table S1), is required for phagolysosome vesiculation.

As mammalian ARL8 uses PKHM2 to bind kinesin-1[15], we examined potential PLEKHM family proteins for a role in phagolysosome resolution. A BLAST search with human PKHM2 identified CUP-14 with a 47% similar RUN domain, part of the N-terminal region that binds kinesin-1[15,38] (Figure S7A-B), and T10B10.3 as having a 59% similar internal region. CUP-14 has a C-terminal zinc finger domain similar to PKHM1/3[39], which have been shown to act as a dual effector for ARL8B and RAB7A during lysosomal fusion[40,41]. Phagolysosome vesiculation was not decreased and cargo disappearance was not significantly delayed in *cup-14(cd32)* mutants, even after treatment with *cup-14* RNAi (Figure S7D-E), suggesting that CUP-14 is not an ARL-8 effector during phagolysosomal vesiculation or degradation. In contrast, uncharacterized T10B10.3 has an N-terminal RUN domain and a C-terminal PH domain like PKHM2 (Figure S7A-C). Phagolysosome vesiculation was decreased two-fold and cargo disappearance was delayed over an hour in *T10B10.3(ok2184)* deletion mutants (Figure 6B-D), suggesting that T10B10.3 could be the functional homolog of PKHM2 connecting ARL-8 to Kinesin-1 for phagolysosome tubulation. Therefore, we named T10B10.3 PKHM-2.

The ARL-8 effector HOPS is required for rapid degradation of phagolysosomal vesicles

The vesicle-tethering HOPS complex is an effector of mammalian ARL8 involved in lysosomal degradation by regulating fusion with lysosomes[42]. As the HOPS subunit VPS41 binds ARL8B[43], we asked whether VPS-41 is required for phagolysosome vesiculation. RNAi knockdown of *vps-41* did not affect phagolysosome vesiculation (Figure 6E) but significantly delayed the degradation of polar body cargo (Fig. 6D, F), specifically delaying the disappearance of phagolysosomal vesicles after vesiculation (Figure 6G). Given that HOPS promotes lysosome fusion[44], HOPS depletion likely affects fusion of small phagolysosomal vesicles to additional lysosomes to promote cargo breakdown. However, *vps-41* knockdown had no effect on polar body membrane breakdown within the large phagolysosome (Figure 6H), an earlier process that depends on RAB-7-mediated phagosome-lysosome fusion[4]. These data suggest that the requirement for HOPS during lysosome fusion may depend on the target vesicle.

Discussion

Using an *in vivo* system to analyze the dynamics of single phagolysosomes containing a physiological cargo, we uncovered the timing and molecular mechanisms of phagolysosome resolution. Digestion of corpse cargo by lysosomal hydrolases starts after fusion of phagosomes to lysosomes and after breakdown of the corpse membrane inside the

phagolysosome[4]. Degradation of cargo proteins by lysosomal hydrolases generates free amino acids within the phagolysosome that are then exported by solute carriers, including SLC-36.1. Amino acids or other breakdown products could then recruit and activate TORC1 on the phagolysosome surface (Figure 7A-B), where it can relieve inhibition of BORC by Ragulator. Independent of TORC1 and Ragulator, BORC recruits the small GTPase ARL-8 to the phagolysosome (Figure 7B), likely in its nucleotide-free form[18]. Based on the ability of SAM-4 to promote GTP exchange[18], we predict that BORC promotes GTP binding of ARL-8 (Figure 7B). ARL-8 then needs to cycle between a GTP-, GDP-, and unbound state to dynamically link the phagolysosomal membrane to kinesin-1 through the PLEKHM2-like protein PKHM-2 to extend tubules and release phagolysosomal vesicles (Figure 7C). The released vesicles then depend on lysosomal fusion mediated by the HOPS tethering complex to facilitate cargo degradation and compartment resolution (Figure 7D).

We discovered many molecular details of the TORC1-BORC-ARL8 pathway of phagolysosomal tubulation, but also revealed hints that there are multiple pathways regulating phagolysosomal vesiculation. First, we still observed vesiculation events in BORC deletion mutants in both *C. elegans* embryonic blastomeres and mammalian macrophages (Figure 2), suggesting that there are BORC-independent pathways promoting vesiculation. We also observed that *slc-36.1* knockdown was able to disrupt phagolysosome vesiculation in the *blos-7(L30A)* mutant (Figure 2D), suggesting that neutral amino acid export from the phagolysosome can do more than activate TORC1 and relieve BORC inhibition by Ragulator. However, *slc-36.1* knockdown was not able to further reduce the number of vesiculation events in *blos-7* deletion mutants (Figure 2E), raising the possibility that the SLC-36.1 pathway converges into the TORC1-BORC-ARL8 pathway downstream of BORC inhibition and independent of ARL-8 localization. Identification of additional factors in the SLC-36.1 pathway will illuminate the distinctions and commonalities between these pathways. In addition, given that TORC1 can respond to signals other than amino acids[45], it will be important to determine which catabolites of phagolysosomal cargos activate proteins upstream of TORC1.

We discovered that phagolysosome tubulation uses similar TORC1-BORC-ARL8 machineries as lysosome trafficking (Table S1)[16-19]. One possible distinction between lysosomal movement and tubulation are that vesiculation forces pull the phagolysosome in opposite directions, which could be accomplished by different microtubule motors. Indeed, endolysosomes can interact with minus-end-directed dynein motors via ARL8[46,47], in addition to plus-end-directed kinesins. The use of multiple motors by ARL-8 could explain why we observed a milder tubulation phenotype disrupting PKHM-2 and the kinesin UNC-116 than disrupting ARL-8. Alternatively, an organelle could hold the phagolysosome to prevent its movement and allow microtubule motors to deform the phagolysosome for tubulation. One possibility is that ER-phagolysosome contacts hold the phagolysosome in place to enable tubulation[28]. These possibilities are not mutually exclusive.

Although BORC and ARL-8 act downstream of TORC1 in phagolysosomal tubulation, we did not observe mislocalization of ARL-8 in embryos deficient for amino acid transporters, Ragulator, or TORC1. In the absence of nutrients, Ragulator is thought to keep BORC and ARL8 away from kinesin motor proteins that transport lysosomes towards the cell

surface[20,21], but not to influence ARL8 localization to the lysosome. If the sole role of TORC1 activation in tubulation is to release BORC inhibition by Ragulator without disrupting Ragulator, as suggested by our BLOS-7(L30A) and *lmtr-2* deletion mutant experiments, what is the molecular function of disinhibited BORC and what else is Ragulator doing? Our data suggests that relieving BORC inhibition or deleting Ragulator does not regulate ARL-8 localization, which further suggests they are not promoting GTP exchange for ARL-8. Whether TORC1 activating BORC through Ragulator alters the dynamics of ARL-8 through its GTPase activity or acts through another downstream interactor remains unclear.

Small GTPase localization is often guided by a localized GEF, which recruits and promotes membrane association of the GTPase[48]. However, we observed that GTP-locked ARL-8(Q75L) localizes non-specifically to membrane compartments but fails to enrich on lysosomes, revealing that GTP-association is not sufficient to enrich ARL-8 on lysosomes. This is likely due to SAM-4 binding to nucleotide-free ARL-8[18] and being unable to recruit GTP-locked ARL-8(Q75L). Similarly, SAM-4 is unable to stably recruit ARL-8 G4 motif mutants to lysosomes, likely because nucleotide-binding of G4 motif mutants is weakened[49], such that they cannot stably bind GTP or GDP. Thus, SAM-4 binding to nucleotide-free ARL-8 and the ability to remain GTP-bound may be necessary to localize ARL-8 specifically to lysosomes and phagolysosomes.

The early endosomal localization of ARL-8 also suggests the presence of an early endosomal GEF that promotes endosomal membrane binding. This Arl GEF is unlikely to be BORC because we observed ARL-8 accumulating on enlarged RAB-5-positive endosomes in BORC mutants. RAB-5 endosomes are enlarged upon interfering with ARL-8-lysosome association or the GDP-GTP cycle of ARL-8, suggesting that ARL-8 may need to be turned over on early endosomes to allow endosome maturation. These giant early endosomes resemble those formed in GTP-locked Rab5(Q79L) mutants[50], which also stably localize to early endosomes and disrupt endosome maturation. Intriguingly, cell corpse phagosomes colocalized with RAB-5 for slightly longer in strong *arl-8* loss-of-function mutants[34], suggesting that ARL-8 may also promote Rab turnover for the maturation of early phagosomes and early endosomes.

By studying single phagosomes over their lifetimes, we uncovered how large phagolysosomes tubulate to form smaller vesicles and facilitate degradation. The ARL-8 effector HOPS likely promotes degradation of phagolysosomal vesicles via its role in lysosome fusion[44], suggesting that multiple rounds of lysosome fusion are required for degradation of phagolysosomal cargo. We propose that HOPS binds to ARL-8-GTP on phagolysosome vesicles to promote lysosome fusion (Figure 7D), but it could interact with another protein independent of ARL-8. Phagolysosomal degradation begins with RAB-7-mediated fusion of the large phagosome with lysosomes to allow the cargo membrane to be broken down[4] and continues with HOPS-mediated fusion of small phagolysosomal vesicles with lysosomes. It will be important to determine why different proteins are required for lysosome fusion to different vesicles containing similar cargo.

Given the difficulty in unambiguously tracking a single phagosome in mammalian cells, let alone mammals, clearance of the *C. elegans* polar body is a powerful *in vivo* system to better understand the factors involved in phagolysosome resolution. mTOR was previously shown to be required for fragmentation of phagocytic and entotic cargo in both *C. elegans* and mammals[4,5], and we discovered that disrupting BORC subunits prevented phagolysosome fragmentation in both worms and mammals. Thus, evolutionarily conserved mechanisms conduct phagolysosome resolution. Given the importance of effectively resolving phagolysosomes containing pathogens or cell corpses, we predict that this pathway has a critical impact on the modulation of immune responses as well as metabolism.

STAR Methods

Resource availability

Lead contact—Further information and requests for resources and reagents should be directed to and will be fulfilled by the lead contact, Gholamreza Fazeli <gholamreza.fazeli@uni-wuerzburg.de>.

Materials availability—All *C. elegans* strains and plasmids generated for this study are available upon request to the lead contact.

Data and code availability

- Microscopy data reported in this paper will be shared by the lead contact upon request.
- This paper does not report original code.
- Any additional information required to reanalyze the data reported in this paper is available from the lead contact upon request.

Experimental model and subject details

Worm strains and maintenance—The nematode *C. elegans* was used for most studies and grown at room temperature according to standard procedures[54]. All *C. elegans* strains used are detailed in the key resources table. Male and hermaphrodite worms were used for genetic crosses. Unmated hermaphrodite worms were dissected to obtain embryos. The sex of embryos was not determined but likely to be hermaphrodite.

Mammalian cell culture—The murine macrophage J774 cell line was used for the data in Figure 2F-I. Cells were cultured according to standard protocol in DMEM supplemented with 100 U/ml penicillin, 100 μg/ml streptomycin, and 10% heat-inactivated fetal bovine serum. Cells were passaged by scraping when they reached 80 – 90% confluency.

No human subjects or mice were included in the study.

Method details

C. elegans genome editing—CRISPR mutations and fluorescent protein knock-ins were ordered from SunyBiotech. Germline-optimized mCitrine[59] was synthesized by Eurofins and

inserted before the stop codon of *arl-8* or *unc-116* with a 20 amino acid flexible linker. Germline-optimized mScarlet-I was amplified from pMS51[60] and inserted before the stop codon of *sam-4* with a 20 amino acid flexible linker. A codon-optimized ZF1 degron tag[61] was inserted directly before the stop codon in *unc-116::mCitrine* or *sam-4::mScarlet-I*. The ARL-8::mCitrine knock-in did not alter developmental timing, viability, or fertility. While ARL-8(T34N) mutants were also viable and fertile, the combination of the mCitrine tag with the T34N mutation led to maternal-effect embryonic lethality in ARL-8(T34N)::mCit worms, similar to the strong loss-of-function deletion allele *tm2504*, suggesting that both perturbations partially disrupt ARL-8 function.

Worm genotyping and phenotyping—Worms were PCR genotyped using primers in key resources table. Restriction fragment length polymorphisms (RFLP) using the following restriction enzymes were performed: *arl-8(jpn1)* with MboII, *arl-8(syb3658D133A)* with NlaIV, *arl-8(syb2255Q75L)* with Hpy188I, *ari-8(syb2260T34N)* with BstXI, *blos-7(syb6675L30A)* with SalI, *bios-8(js1354)* with HinDIII, *blos-9(js1352)* with Bell, *cup-14(cd32)* with PstI. *glo-2* mutants were phenotyped on a DM5500 wide-field fluorescence microscope (Leica) by the absence of auto-fluorescent and birefringent gut granules. *unc-104(e1265)* mutants were phenotyped by severe paralysis.

RNAi experiments—RNAi was performed by feeding dsRNA-expressing bacteria at 25°C from the L1 larval stage through adulthood (64-72 hours) according to established protocols[62]. RNAi constructs were published previously (*daf-15* and *rict-1* RNAi[51]) or were obtained from available libraries (Source BioScience, *let-363 (sjj2_B0261.2a), rab-7 (mv_E03C9.3), slc-36.1 (sjj_Y43F4B.7), and vps-41 (sjj2_F32A6.3)*).

Light Microscopy—Embryos dissected on a cover slip in M9 buffer were mounted on a slide on top of an agarose pad. Sixteen 1.2 pm step Z-stacks were acquired sequentially for (GFP and) mCherry and DIC every minute at room temperature using a DM5500 wide-field fluorescence microscope with a HC PL APO 40X 1.3 NA oil objective lens supplemented with a DFC365 FX CCD camera controlled by LAS AF software (Leica). Confocal images were obtained using a Leica SP5 confocal with a HCX PL APO CS 63x 1.4 NA oil objective with Leica HyD hybrid detectors. To image ARL-8::mCit localization, dissected embryos were transferred into egg salts in a 4- or 8-chamber glass bottom slide (ibidi), illuminated using a Tilt light sheet (Mizar), and imaged using an Axio Observer 7 (Zeiss) with a 40X 1.4 NA oil objective lens and ORCA-Fusion sCMOS camera (Hamamatsu) controlled by SlideBook software (3i).

Image Analysis—Time-lapse series were analyzed using Imaris (Oxford Instruments). Internalization was defined as the first frame where the polar body moves away from the plasma membrane, which is likely to closely reflect closure of the phagocytic cup. Vesiculation events were scored when the vesicles were clearly distinct from each other, likely underestimating budding events. Each vesicle was followed individually until disappearance. Degradation was defined as the last frame where mCh reporters were observed after examining the following five frames for mCh puncta reappearance. A

maximum of 170 min past engulfment was considered as the end of each time lapse if the phagolysosome was not yet degraded.

Colocalization analysis—z-stacks of 1-4-cell embryos where deconvolved and smoothened using a median filter to reduce the noise and the background was masked in Imaris. For each channel, surfaces were created to annotate the fluorescent structures using 3D View in Imaris. Thresholded colocalization of ARL-8::mCit with SAM-4::mSc or mCh::RAB-5 was measured using the Coloc tool of Imaris and percent of ARL-8 colocalization and Pearson coefficient in colocalized volume was reported.

Antibody staining—Gravid worms were dissected in water on a coverslip to release embryos and transferred to 0.1% polylysine-coated slides and frozen on dry ice. Eggshells were cracked by flicking off the coverslip and embryos were fixed in methanol before staining. The following antibodies were used: mouse α-LMP-1 antibody (1:50, AB_2161795, Developmental Studies Hybridoma Bank), chicken α-GFP (1:500, AB_2307313, Aves). Slides were counterstained with DAPI to label DNA and mounted using DABCO.

Image processing—For clarity, images were rotated, colorized and the intensity was adjusted using Adobe Photoshop. All images show a single optical section (Z), except Figure 1D, where the last two panels are maximum projection of two Zs with 1.2 μm steps. Several Zs with 1.2 μm steps were maximum projected in Imaris for videos.

Generation of mutant macrophage clones—Cas9-expressing J774 cells were transduced with lentivirus based on pMCB320 (Addgene plasmid #89359) with mCherry replaced by BFP and containing the sgRNA sequences given in the key resources table. Two days after transduction, sgRNA-expressing cells were selected with puromycin (2 pgμg/ml). CRISPR-modified J774 cells were isolated to identify clonal lines. Genomic DNA from clones was PCR amplified, sequenced, and subjected to TIDE analysis to verify genome edits[63] (Figure S2).

Fragmentation assay—J774 cells were plated on coverslips in 12-well plates (75,000 cells/well) for 24 hours. Sheep red blood cells (SRBC) were opsonized with rabbit anti-sheep IgG (MP Biomedical) as described[64] and labeled with TAMRA-succinimidyl ester. Macrophages were fed IgG-coated SRBCs at a ratio of 3 SRBC per macrophage for 30 minutes, washed with D-PBS, placed in fresh culture media, and incubated at 37°C for 6 h. J774 cells were then washed with D-PBS and fixed with 2% PFA for 12 min before imaging on a confocal microscope. The extent of phagolysosome fragmentation was scored (Stage I-III) for >120 cells in three separate experiments using the same clonal cell lines.

Quantification and Statistical analysis

Student's one-tailed *t*-test (Microsoft Excel), or Chi-squared test (Graph Pad Prism) were used to test statistical significance using the Bonferroni correction to adjust for multiple comparisons. Statistical analysis used for each experiment and p-values are given in figure legends. Each circle in graphs represents one phagolysosome of an embryo. Therefore, the

number of circles denotes the n in each experiment. Mean ± standard error of the mean is depicted in graphs and text, except for Figure 2I, where mean ± standard deviation is shown.

Supplementary Material

Refer to Web version on PubMed Central for supplementary material.

Acknowledgements

Anna Henrich, Martin Boos, Kaitlyn Spees, Jasmine Garcia, Heather Chorzempa, Lauren Pitts and Riley Harrison provided technical assistance. The authors thank the RVZ imaging facility for imaging and data analysis support. Strains, constructs, and reagents were generously provided by Ralf Baumeister, Hanna Fares, Greg Hermann, Shinsuke Niwa, Michael Nonet, Karen Oegema, Kang Shen, the Japan National Bioresource Project (NBRP), and the Caenorhabditis Genetics Center (CGC), which is funded by NIH Office of Research Infrastructure Programs (P40 OD010440). Todd Blankenship, Julia Frondoni, Shruti Kolli, Alex Nguyen, and anonymous reviewers provided valuable comments on the manuscript. This work was funded by Deutsche Forschungsgemeinschaft (DFG) grants FA1046/3-1 to G.F. and STI700/1-1 to C.S. and NIH grant R15 GM143727-01 to A.M.W. & G.F.

Inclusion and Diversity

We support inclusive, diverse, and equitable conduct of research.

References

1. Fond AM, and Ravichandran KS (2016). Clearance of Dying Cells by Phagocytes: Mechanisms and Implications for Disease Pathogenesis. Adv Exp Med Biol 930, 25–49. 10.1007/978-3-319-39406-0_2. [PubMed: 27558816]
2. Ghose P, and Wehman AM (2021). The developmental and physiological roles of phagocytosis in Caenorhabditis elegans. Curr Top Dev Biol 144, 409–432. 10.1016/bs.ctdb.2020.09.001. [PubMed: 33992160]
3. Doran AC, Yurdagul A Jr., and Tabas I (2020). Efferocytosis in health and disease. Nat Rev Immunol 20, 254–267. 10.1038/s41577-019-0240-6. [PubMed: 31822793]
4. Fazeli G, Stetter M, Lisack JN, and Wehman AM (2018). C. elegans Blastomeres Clear the Corpse of the Second Polar Body by LC3-Associated Phagocytosis. Cell Rep 23, 2070–2082. 10.1016/j.celrep.2018.04.043. [PubMed: 29768205]
5. Krajcovic M, Krishna S, Akkari L, Joyce JA, and Overholtzer M (2013). mTOR regulates phagosome and entotic vacuole fission. Mol Biol Cell 24, 3736–3745. 10.1091/mbc.E13-07-0408. [PubMed: 24088573]
6. Abdu Y, Maniscalco C, Heddleston JM, Chew TL, and Nance J (2016). Developmentally programmed germ cell remodelling by endodermal cell cannibalism. Nat Cell Biol 18, 1302–1310. 10.1038/ncb3439. [PubMed: 27842058]
7. Melentijevic I, Toth ML, Arnold ML, Guasp RJ, Harinath G, Nguyen KC, Taub D, Parker JA, Neri C, Gabel CV, et al. (2017). C-elegans neurons jettison protein aggregates and mitochondria under neurotoxic stress. Nature 542, 367-+. 10.1038/nature21362. [PubMed: 28178240]
8. Yu L, McPhee CK, Zheng L, Mardones GA, Rong Y, Peng J, Mi N, Zhao Y, Liu Z, Wan F, et al. (2010). Termination of autophagy and reformation of lysosomes regulated by mTOR. Nature 465, 942–946. 10.1038/nature09076. [PubMed: 20526321]
9. Gan Q, Wang X, Zhang Q, Yin Q, Jian Y, Liu Y, Xuan N, Li J, Zhou J, Liu K, et al. (2019). The amino acid transporter SLC-36.1 cooperates with PtdIns3P 5-kinase to control phagocytic lysosome reformation. J Cell Biol 218, 2619–2637. 10.1083/jcb.201901074. [PubMed: 31235480]
10. Lancaster CE, Fountain A, Dayam RM, Somerville E, Sheth J, Jacobelli V, Somerville A, Terebiznik MR, and Botelho RJ (2021). Phagosome resolution regenerates lysosomes and maintains the degradative capacity in phagocytes. J Cell Biol 220. 10.1083/jcb.202005072.

11. Saxton RA, and Sabatini DM (2017). mTOR Signaling in Growth, Metabolism, and Disease. Cell 169, 361–371. 10.1016/j.cell.2017.03.035.
12. Khatter D, Sindhwani A, and Sharma M (2015). Arf-like GTPase Arl8: Moving from the periphery to the center of lysosomal biology. Cell Logist 5, e1086501. 10.1080/21592799.2015.1086501. [PubMed: 27057420]
13. Klassen MP, Wu YE, Maeder CI, Nakae I, Cueva JG, Lehrman EK, Tada M, Gengyo-Ando K, Wang GJ, Goodman M, et al. (2010). An Arf-like small G protein, ARL-8, promotes the axonal transport of presynaptic cargoes by suppressing vesicle aggregation. Neuron 66, 710–723. 10.1016/j.neuron.2010.04.033. [PubMed: 20547129]
14. Niwa S, Lipton DM, Morikawa M, Zhao C, Hirokawa N, Lu H, and Shen K (2016). Autoinhibition of a Neuronal Kinesin UNC-104/KIF1A Regulates the Size and Density of Synapses. Cell Rep 16, 2129–2141. 10.1016/j.celrep.2016.07.043. [PubMed: 27524618]
15. Rosa-Ferreira C, and Munro S (2011). Arl8 and SKIP act together to link lysosomes to kinesin-1. Dev Cell 21, 1171–1178. 10.1016/j.devcel.2011.10.007. [PubMed: 22172677]
16. Pu J, Schindler C, Jia R, Jarnik M, Backlund P, and Bonifacino JS (2015). BORC, a multisubunit complex that regulates lysosome positioning. Dev Cell 33, 176–188. 10.1016/j.devcel.2015.02.011. [PubMed: 25898167]
17. Farias GG, Guardia CM, De Pace R, Britt DJ, and Bonifacino JS (2017). BORC/kinesin-1 ensemble drives polarized transport of lysosomes into the axon. Proc Natl Acad Sci U S A 114, E2955–E2964. 10.1073/pnas.1616363114. [PubMed: 28320970]
18. Niwa S, Tao L, Lu SY, Liew GM, Feng W, Nachury MV, and Shen K (2017). BORC Regulates the Axonal Transport of Synaptic Vesicle Precursors by Activating ARL-8. Curr Biol 27, 2569–2578 e2564. 10.1016/j.cub.2017.07.013. [PubMed: 28823680]
19. De Pace R, Britt DJ, Mercurio J, Foster AM, Djavaherian L, Hoffmann V, Abebe D, and Bonifacino JS (2020). Synaptic Vesicle Precursors and Lysosomes Are Transported by Different Mechanisms in the Axon of Mammalian Neurons. Cell Rep 31, 107775. 10.1016/j.celrep.2020.107775. [PubMed: 32553155]
20. Filipek PA, de Araujo MEG, Vogel GF, De Smet CH, Eberharter D, Rebsamen M, Rudashevskaya EL, Kremser L, Yordanov T, Tschaikner P, et al. (2017). LAMTOR/Ragulator is a negative regulator of Arl8b- and BORC-dependent late endosomal positioning. J Cell Biol 216, 4199–4215. 10.1083/jcb.201703061. [PubMed: 28993467]
21. Pu J, Keren-Kaplan T, and Bonifacino JS (2017). A Ragulator-BORC interaction controls lysosome positioning in response to amino acid availability. J Cell Biol 216, 4183–4197. 10.1083/jcb.201703094. [PubMed: 28993468]
22. Colaco A, and Jaattela M (2017). Ragulator-a multifaceted regulator of lysosomal signaling and trafficking. J Cell Biol 216, 3895–3898. 10.1083/jcb.201710039. [PubMed: 29138253]
23. Shang P, Valapala M, Grebe R, Hose S, Ghosh S, Bhutto IA, Handa JT, Lutty GA, Lu L, Wan J, et al. (2017). The amino acid transporter SLC36A4 regulates the amino acid pool in retinal pigmented epithelial cells and mediates the mechanistic target of rapamycin, complex 1 signaling. Aging Cell 16, 349–359. 10.1111/acel.12561. [PubMed: 28083894]
24. Heublein S, Kazi S, Ogmundsdottir MH, Attwood EV, Kala S, Boyd CA, Wilson C, and Goberdhan DC (2010). Proton-assisted amino-acid transporters are conserved regulators of proliferation and amino-acid-dependent mTORC1 activation. Oncogene 29, 4068–4079. 10.1038/onc.2010.177. [PubMed: 20498635]
25. Inoki K, Zhu T, and Guan KL (2003). TSC2 mediates cellular energy response to control cell growth and survival. Cell 115, 577–590. 10.1016/s0092-8674(03)00929-2. [PubMed: 14651849]
26. Gwinn DM, Shackelford DB, Egan DF, Mihaylova MM, Mery A, Vasquez DS, Turk BE, and Shaw RJ (2008). AMPK phosphorylation of raptor mediates a metabolic checkpoint. Mol Cell 30, 214–226. 10.1016/j.molcel.2008.03.003. [PubMed: 18439900]
27. Langemeyer L, and Ungermann C (2015). BORC and BLOC-1: Shared subunits in trafficking complexes. Dev Cell 33, 121–122. 10.1016/j.devcel.2015.04.008. [PubMed: 25898163]
28. Levin-Konigsberg R, Montano-Rendon F, Keren-Kaplan T, Li R, Ego B, Mylvaganam S, DiCiccio JE, Trimble WS, Bassik MC, Bonifacino JS, et al. (2019). Phagolysosome resolution requires

contacts with the endoplasmic reticulum and phosphatidylinositol-4-phosphate signalling. Nat Cell Biol 21, 1234–1247. 10.1038/s41556-019-0394-2. [PubMed: 31570833]

29. Sancak Y, Bar-Peled L, Zoncu R, Markhard AL, Nada S, and Sabatini DM (2010). Ragulator-Rag complex targets mTORC1 to the lysosomal surface and is necessary for its activation by amino acids. Cell 141, 290–303. 10.1016/j.cell.2010.02.024. [PubMed: 20381137]
30. Bar-Peled L, Schweitzer LD, Zoncu R, and Sabatini DM (2012). Ragulator is a GEF for the rag GTPases that signal amino acid levels to mTORC1. Cell 150, 1196–1208. 10.1016/j.cell.2012.07.032. [PubMed: 22980980]
31. Bagshaw RD, Callahan JW, and Mahuran DJ (2006). The Arf-family protein, Arl8b, is involved in the spatial distribution of lysosomes. Biochem Biophys Res Commun 344, 1186–1191. 10.1016/j.bbrc.2006.03.221. [PubMed: 16650381]
32. Nakae I, Fujino T, Kobayashi T, Sasaki A, Kikko Y, Fukuyama M, Gengyo- Ando K, Mitani S, Kontani K, and Katada T (2010). The arf-like GTPase Arl8 mediates delivery of endocytosed macromolecules to lysosomes in Caenorhabditis elegans. Mol Biol Cell 21, 2434–2442. 10.1091/mbc.E09-12-1010. [PubMed: 20484575]
33. Morris C, Foster OK, Handa S, Peloza K, Voss L, Somhegyi H, Jian Y, Vo MV, Harp M, Rambo FM, et al. (2018). Function and regulation of the Caenorhabditis elegans Rab32 family member GLO-1 in lysosome-related organelle biogenesis. PLoS Genet 14, e1007772. 10.1371/journal.pgen.1007772. [PubMed: 30419011]
34. Sasaki A, Nakae I, Nagasawa M, Hashimoto K, Abe F, Saito K, Fukuyama M, Gengyo-Ando K, Mitani S, Katada T, and Kontani K (2013). Arl8/ARL-8 functions in apoptotic cell removal by mediating phagolysosome formation in Caenorhabditis elegans. Mol Biol Cell 24, 1584–1592. 10.1091/mbc.E12-08-0628. [PubMed: 23485564]
35. Thompson A, Jannoo R, and Kanamarlapudi V (2018). Arl8b. In Encyclopedia of Signaling Molecules, Choi S, ed. (Springer International Publishing), pp. 430–436. 10.1007/978-3-319-67199-4_400.
36. Armenti ST, Lohmer LL, Sherwood DR, and Nance J (2014). Repurposing an endogenous degradation system for rapid and targeted depletion of C. elegans proteins. Development 141, 4640–4647. 10.1242/dev.115048. [PubMed: 25377555]
37. Yang HY, Mains PE, and McNally FJ (2005). Kinesin-1 mediates translocation of the meiotic spindle to the oocyte cortex through KCA-1, a novel cargo adapter. J Cell Biol 169, 447–457. 10.1083/jcb.200411132. [PubMed: 15883196]
38. Boucrot E, Henry T, Borg JP, Gorvel JP, and Meresse S (2005). The intracellular fate of Salmonella depends on the recruitment of kinesin. Science 308, 1174–1178. 10.1126/science.1110225. [PubMed: 15905402]
39. Gee K, Zamora D, Horm T, George L, Upchurch C, Randall J, Weaver C, Sanford C, Miller A, Hernandez S, et al. (2017). Regulators of Lysosome Function and Dynamics in Caenorhabditis elegans. G3 (Bethesda) 7, 991–1000. 10.1534/g3.116.037515. [PubMed: 28122949]
40. Marwaha R, Arya SB, Jagga D, Kaur H, Tuli A, and Sharma M (2017). The Rab7 effector PLEKHM1 binds Arl8b to promote cargo traffic to lysosomes. J Cell Biol 216, 1051–1070. 10.1083/jcb.201607085. [PubMed: 28325809]
41. McEwan DG, Popovic D, Gubas A, Terawaki S, Suzuki H, Stadel D, Coxon FP, de Stegmann DM, Bhogaraju S, Maddi K, et al. (2015). PLEKHM1 Regulates Autophagosome-Lysosome Fusion through HOPS Complex and LC3/GABARAP Proteins. Molecular Cell 57, 39–54. 10.1016/j.molcel.2014.11.006. [PubMed: 25498145]
42. Jia R, Guardia CM, Pu J, Chen Y, and Bonifacino JS (2017). BORC coordinates encounter and fusion of lysosomes with autophagosomes. Autophagy 13, 1648–1663. 10.1080/15548627.2017.1343768. [PubMed: 28825857]
43. Khatter D, Raina VB, Dwivedi D, Sindhwani A, Bahl S, and Sharma M (2015). The small GTPase Arl8b regulates assembly of the mammalian HOPS complex on lysosomes. J Cell Sci 128, 1746–1761. 10.1242/jcs.162651. [PubMed: 25908847]
44. Nguyen JA, and Yates RM (2021). Better Together: Current Insights Into Phagosome-Lysosome Fusion. Front Immunol 12, 636078. 10.3389/fimmu.2021.636078. [PubMed: 33717183]

45. Dokudovskaya S, and Rout MP (2015). SEA you later alli-GATOR--a dynamic regulator of the TORC1 stress response pathway. J Cell Sci 128, 2219–2228. 10.1242/jcs.168922. [PubMed: 25934700]
46. Keren-Kaplan T, Saric A, Ghosh S, Williamson CD, Jia R, Li Y, and Bonifacino JS (2022). RUFY3 and RUFY4 are ARL8 effectors that promote coupling of endolysosomes to dynein-dynactin. Nat Commun 13, 1506. 10.1038/s41467-022-28952-y. [PubMed: 35314674]
47. Kumar G, Chawla P, Dhiman N, Chadha S, Sharma S, Sethi K, Sharma M, and Tuli A (2022). RUFY3 links Arl8b and JIP4-Dynein complex to regulate lysosome size and positioning. Nat Commun 13, 1540. 10.1038/s41467-022-29077-y. [PubMed: 35314681]
48. Blumer J, Rey J, Dehmelt L, Mazel T, Wu YW, Bastiaens P, Goody RS, and Itzen A (2013). RabGEFs are a major determinant for specific Rab membrane targeting. J Cell Biol 200, 287–300. 10.1083/jcb.201209113. [PubMed: 23382462]
49. McCray BA, Skordalakes E, and Taylor JP (2010). Disease mutations in Rab7 result in unregulated nucleotide exchange and inappropriate activation. Hum Mol Genet 19, 1033–1047. 10.1093/hmg/ddp567. [PubMed: 20028791]
50. Stenmark H, Parton RG, Steele-Mortimer O, Lutcke A, Gruenberg J, and Zerial M (1994). Inhibition of rab5 GTPase activity stimulates membrane fusion in endocytosis. EMBO J 13, 1287–1296. [PubMed: 8137813]
51. Qi W, Yan Y, Pfeifer D, Donner VGE, Wang Y, Maier W, and Baumeister R (2017). C. elegans DAF-16/FOXO interacts with TGF-ss/BMP signaling to induce germline tumor formation via mTORC1 activation. PLoS Genet 13, e1006801. 10.1371/journal.pgen.1006801. [PubMed: 28549065]
52. Kamber RA, Nishiga Y, Morton B, Banuelos AM, Barkal AA, Vences-Catalan F, Gu M, Fernandez D, Seoane JA, Yao D, et al. (2021). Inter-cellular CRISPR screens reveal regulators of cancer cell phagocytosis. Nature 597, 549–554. 10.1038/s41586-021-03879-4. [PubMed: 34497417]
53. Hermann GJ, Schroeder LK, Hieb CA, Kershner AM, Rabbitts BM, Fonarev P, Grant BD, and Priess JR (2005). Genetic analysis of lysosomal trafficking in Caenorhabditis elegans. Mol Biol Cell 16, 3273–3288. 10.1091/mbc.e05-01-0060. [PubMed: 15843430]
54. Brenner S (1974). The genetics of Caenorhabditis elegans. Genetics 77, 71–94. [PubMed: 4366476]
55. Audhya A, McLeod IX, Yates JR, and Oegema K (2007). MVB-12, a fourth subunit of metazoan ESCRT-I, functions in receptor downregulation. PLoS One 2, e956. 10.1371/journal.pone.0000956. [PubMed: 17895996]
56. Joseph-Strauss D, Gorjanacz M, Santarella-Mellwig R, Voronina E, Audhya A, and Cohen-Fix O (2012). Sm protein down-regulation leads to defects in nuclear pore complex disassembly and distribution in C. elegans embryos. Dev Biol 365, 445–457. 10.1016/j.ydbio.2012.02.036. [PubMed: 22426005]
57. Beer KB, Rivas-Castillo J, Kuhn K, Fazeli G, Karmann B, Nance JF, Stigloher C, and Wehman AM (2018). Extracellular vesicle budding is inhibited by redundant regulators of TAT-5 flippase localization and phospholipid asymmetry. Proc Natl Acad Sci U S A 115, E1127–E1136. 10.1073/pnas.1714085115. [PubMed: 29367422]
58. Sarov M, Murray JI, Schanze K, Pozniakovski A, Niu W, Angermann K, Hasse S, Rupprecht M, Vinis E, Tinney M, et al. (2012). A genome-scale resource for in vivo tag-based protein function exploration in C. elegans. Cell 150, 855–866. S0092-8674(12)00946-4 [pii] 10.1016/j.cell.2012.08.001. [PubMed: 22901814]
59. Fielmich LE, Schmidt R, Dickinson DJ, Goldstein B, Akhmanova A, and van den Heuvel S (2018). Optogenetic dissection of mitotic spindle positioning in vivo. Elife 7. 10.7554/eLife.38198.
60. Dickinson D, Slabodnick M, Chen A, and Goldstein B (2018). SapTrap assembly of repair templates for Cas9-triggered homologous recombination with a self-excising cassette. MicroPubl Biol 2018. 10.17912/W2KT0N.
61. Redemann S, Schloissnig S, Ernst S, Pozniakowsky A, Ayloo S, Hyman AA, and Bringmann H (2011). Codon adaptation-based control of protein expression in C. elegans. Nat Methods 8, 250–252. 10.1038/nmeth.1565. [PubMed: 21278743]

62. Fraser AG, Kamath RS, Zipperlen P, Martinez-Campos M, Sohrmann M, and Ahringer J (2000). Functional genomic analysis of C. elegans chromosome I by systematic RNA interference. Nature 408, 325–330. 10.1038/35042517. [PubMed: 11099033]

63. Brinkman EK, Chen T, Amendola M, and van Steensel B (2014). Easy quantitative assessment of genome editing by sequence trace decomposition. Nucleic Acids Res 42, e168. 10.1093/nar/gku936. [PubMed: 25300484]

64. Montano F, Grinstein S, and Levin R (2018). Quantitative Phagocytosis Assays in Primary and Cultured Macrophages. Methods Mol Biol 1784, 151–163. 10.1007/978-1-4939-7837-3_15. [PubMed: 29761397]

Highlights

- Large phagolysosomes tubulate into small vesicles to facilitate corpse clearance
- Phagolysosome vesiculation depends on amino acid export and TORC1 activation
- BORC recruits ARL-8 and promotes GTP cycling for vesiculation by kinesin-1
- HOPS promotes rapid cargo degradation in small phagolysosomal vesicles

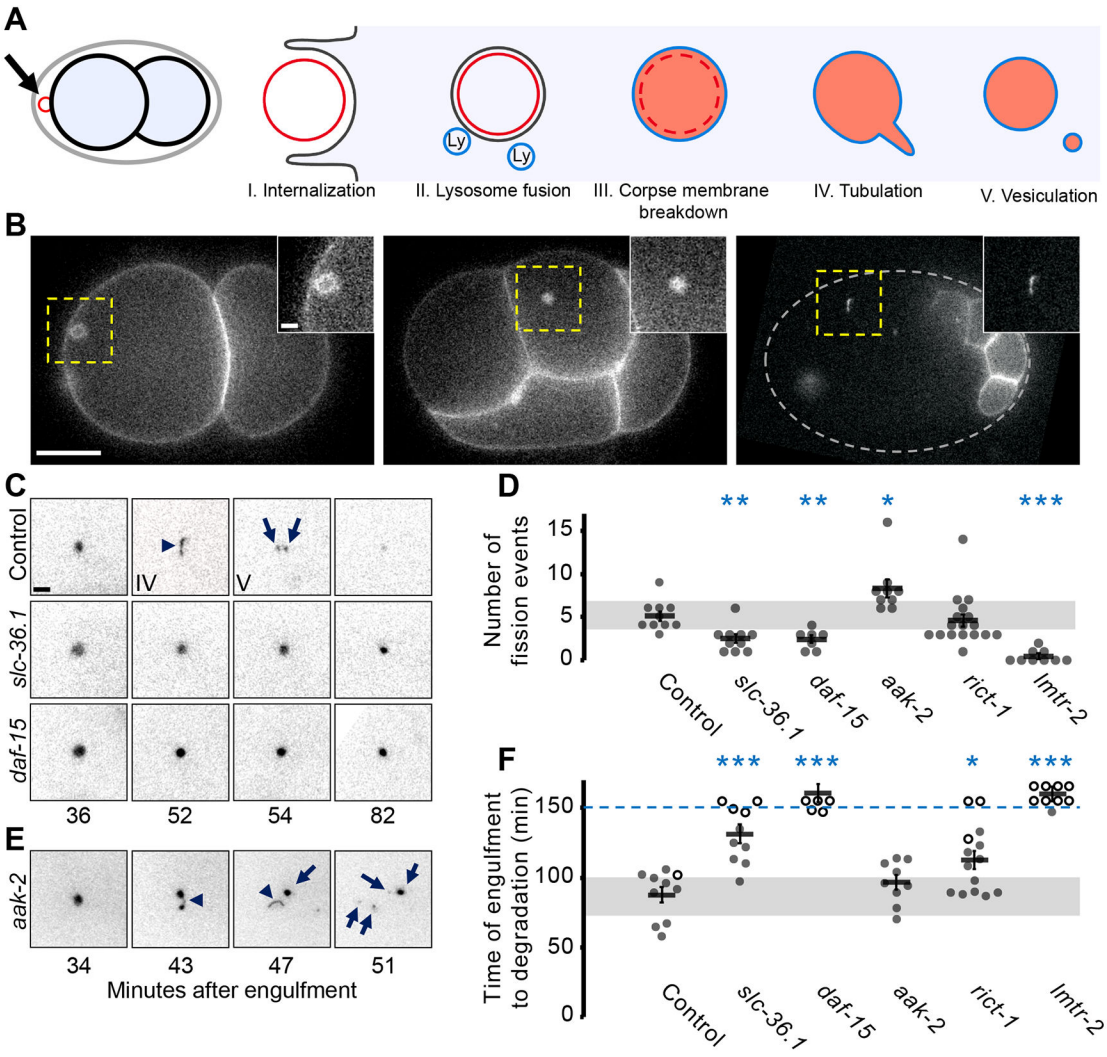

Figure 1: Phagolysosome vesiculation requires amino acid release and TORC1 activation

A) Schematic representation of the fate of the second polar body corpse. The corpse is phagocytosed (I) by a blastomere cell and the phagosome is fused with lysosomes (II). Next the corpse membrane (red) breaks down inside the phagolysosome membrane (blue), dispersing the membrane tag inside the lumen of the phagolysosome (III). Around 40 min later tubules containing cargo are extended from phagolysosome (IV), which then are released as small vesicles (V) to facilitate degradation. B) Representative images of an embryo expressing mCh::PH::ZF1 with a corpse (yellow square) at the stages of internalization (I), corpse membrane breakdown (III) and phagolysosome tubulation (IV). Scale bars in the main panel and magnified inset show 10 and 2 μm respectively. Indicated times are minutes after engulfment. Grey dotted line in the left panel shows the outline of the embryo. See also Figure S1 and Video S1. C) The polar body phagolysosome tubulates (arrowhead) to release vesicles (arrows) in a control embryo, but not after knockdown of the lysosomal amino acid transporter SLC-36.1 or a TORC1 subunit RAPTOR/DAF-15. Panels are inverted for better contrast. D) Fission events are decreased compared to control (5±1) after knockdown of SLC-36.1 (3±0) or DAF-15 (2±0), but not after TORC2 subunit

RICTOR/RICT-1 knockdown (5±1). *aak-2(ok524)* mutants show increased vesiculation (8±1). Fission events were decreased in Ragulator *lmtr-2(tm2367)* mutants (0±0). See also Table S1. E) Disrupting the negative regulator of TORC1, AMPK/AAK-2, results in increased fission events (arrowheads) to produce more phagolysosomal vesicles (arrows). F) The 2nd polar body cargo mCh::PH::ZF1 disappears from the phagolysosome 88±6 min after internalization. Timely disappearance of the corpse cargo depends on SLC-36.1 (131 ±7 min), DAF-15 (>150 min) and RICT-1 (113±7 min). Phagolysosome disappearance was not altered in *aak-2(ok524)* mutants (96±5 min). Disappearance of the phagolysosome cargo was delayed in *lmtr-2(tm2367)* mutants (>150 min). Each circle denotes one phagolysosome. Open circles denote the last frame of a time-lapse series in which the polar body phagolysosome did not disappear. Mean ± SEM is shown. Disappearance times and means beyond 150 min after engulfment are grouped above the dashed blue line. Grey bars show standard deviation of the mean in controls. *p<0.05, **p<0.01, ***p<0.001 compared to control embryos using Student's t-test with Bonferroni correction.

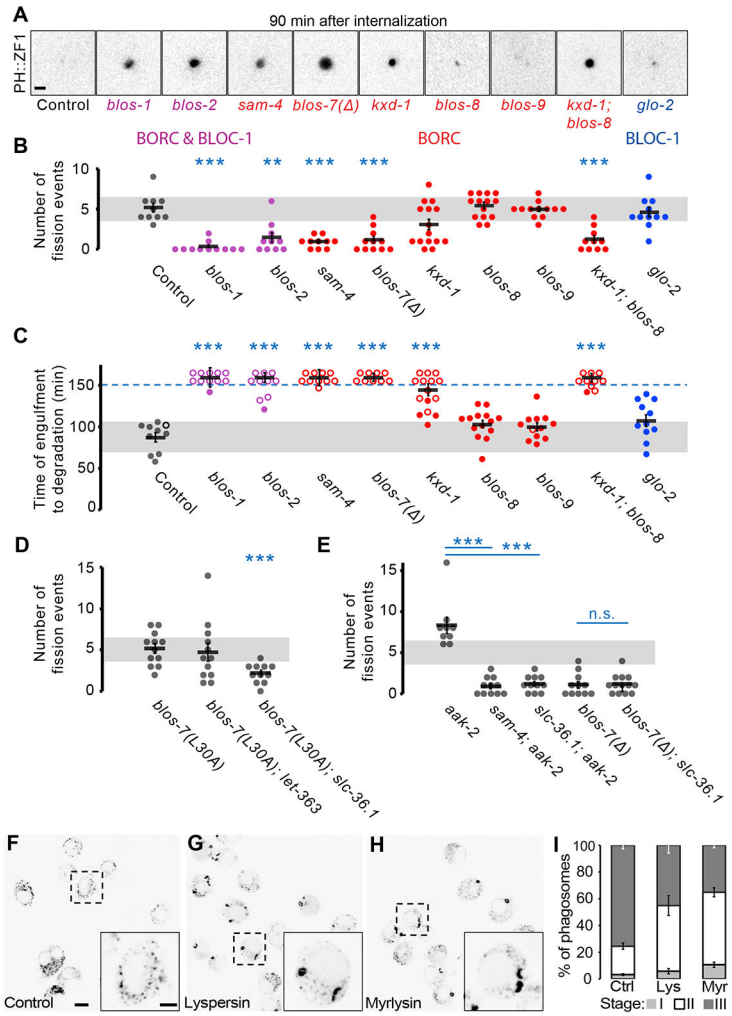

Figure 2: BORC is required for phagolysosome tubulation and cargo degradation in worms and mammals

A) Inverted images of corpse phagolysosomes 90 minutes after engulfment in control and indicated mutants. Scale bar is 2 μm. B) Phagolysosomal fission events were reduced compared to control embryos (5±1) in BORC subunit *blos-1(ok3707)* (0±0), *blos-2(js1351)* (1±1), *sam-4(tm3828)* (1±0), or *blos-7(wy1159)* (1±0) mutants. Single *kxd-1(js1356)* (3±1), *blos-8(js1354)* (5±0) or *blos-9(js 1352)* (5±0) mutants did not significantly decrease fission events, but *kxd-1(js1356); blos-8(js1354)* double mutants decreased fission events (1±0), implying redundancy of some BORC subunits. Disrupting the related complex BLOC-1 with *glo-2(zu455)* mutants did not affect vesiculation (5±1). See also Table S1. C) The 2nd polar body cargo mCh::PH::ZF1 disappears from the phagolysosome 88±6 min after internalization. BORC mutants *blos-1(ok3707)*, *blos-2(js1351)*, *sam-4(tm3828)*, *blos-7(wy1159)* (all >150 min), or *kxd-1(js1356)* (146±7 min), delayed cargo disappearance but not *blos-8(js1354)* (104±5 min) or *blos-9(js1352)* (101±5 min) mutants. Cargo degradation was delayed >150 min in *kxd-1(js1356); blos-8(js1354)* double mutants. Disappearance of the phagolysosome cargo was not affected in *glo-2(zu455)* mutants (108±7 min). See also Video S2. D) Phagolysosomal fission events in *blos-7(L30A)* embryos were not different from control embryos (5–1, p=0.5). Phagolysosomal fission events were

reduced in *blos-7(L30A); slc-36.1* RNAi (2±0) compared to *blos-7(L30A)* embryos, but not in *blos-7(L30A); let-363* RNAi (5±1, p=0.4) mutants. E) Vesiculation was disrupted in *sam-4(tm3828); aak-2(ok524)* double mutants (1±0), and *aak-2(ok524)* mutants treated with *slc-36.1* RNAi (1±0), which were significantly different from *aak-2(ok524)* single mutants (8±1). Phagolysosomal fission events in *blos-7(wy1159); slc-36.1* RNAi (1±0) were not different compared to *blos-7(wy1159)* deletion allele embryos (1±1, p=0.5). Open circles denote the last frame of a time-lapse series in which the polar body phagolysosome did not disappear. Mean ± SEM is shown. Disappearance times and means beyond 150 min after engulfment are grouped above the dashed blue line. Grey bars show standard deviation of the mean in controls. **p<0.01, ***p<0.001 compared to control embryos using Student's t-test with Bonferroni correction, except in 2D, where samples are compared to *blos-7(L30A)* and in 2E, where the comparison pairs are indicated by blue lines. See also Figure S3. F) Murine macrophage J774 cells treated with a control sgRNA engulfed and fragmented opsonized sheep red blood cells (SRBC) within 6 hours after feeding. G-H) Engulfed SRBC remained large with reduced fragmentation in Lyspersin (G) or Myrlysin (H) CRISPR mutant J774 cell lines. See Figure S2 for CRISPR edits. Dotted rectangle is magnified in the insets. Scale bars in the main image and inset are 10 and 5 μm respectively. I) Quantification of phagosome resolution revealed that Lyspersin and Myrlysin mutants significantly decreased stage III (mostly fragmented SRBC, dispersed throughout the cytoplasm) and increased stage I (large, seemingly undigested SRBC) & stage II (large partially digested SRBC with proximal small, fragmented structures). Chi-squared test, p<0.00001. Mean ± SD is shown.

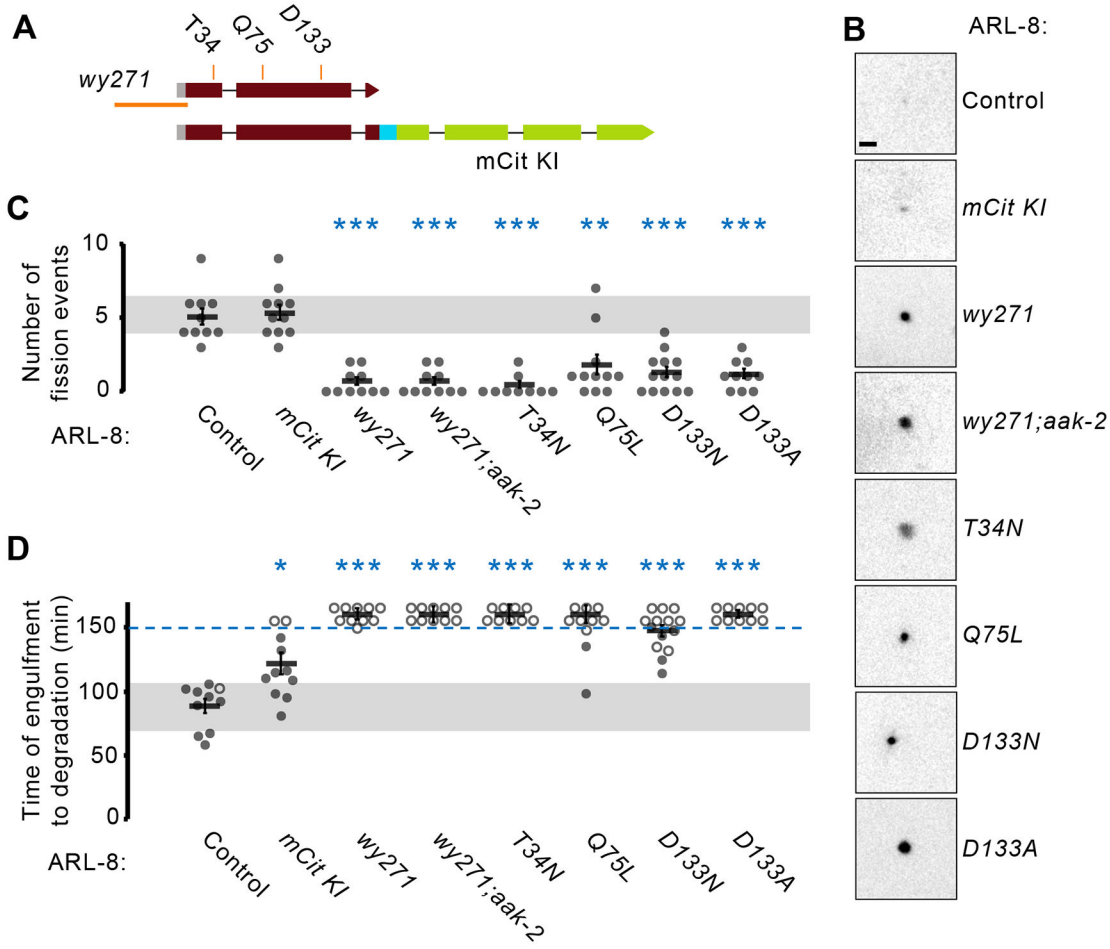

Figure 3: Dysregulating the ARL-8 GTPase cycle disrupts phagolysosome tubulation

A) Genomic *arl-8* locus with *wy271* deletion (orange line) and the point mutations T34N (GDP-bound), Q75L (GTP-bound), D133N and D133A mutations (G4 motif) indicated. mCitrine was inserted in the C-terminus of *arl-8* with a flexible linker (cyan) with or without the above point mutations. B) Inverted images of corpse phagolysosomes 90 minutes after engulfment in control and indicated mutants. Scale bar is 2 μm. C) Knocking mCit into *arl-8* did not affect phagolysosomal fission events (5±1 vs. 5±1 in controls), while fission events were dramatically reduced in *arl-8(wy271)* (1±0), *T34N* (0±0), *Q75L* (2±1), *D133N* (1±0) or *D133A* (1±0) mutants. Vesiculation was also disrupted in *arl-8(wy271); aak-2(ok524)* double mutants (1±0), which was significantly different from *aak-2(ok524)* mutants ($p<0.001$). D) The ARL-8::mCit knock-in slightly delayed the disappearance of the 2nd polar body phagolysosome cargo marker mCh::PH::ZF1 (120±8 min), compared to control (88±6 min), whereas cargo degradation was severely delayed in *arl-8(wy271)*, *T34N*, *Q75L*, *D133A* (all >150 min) or *D133N* (146±4) mutants, as well as *arl-8(wy271); aak-2(ok524)* double mutants (>150 min). Open circles denote the last frame of a time-lapse series in which the polar body phagolysosome did not disappear. Mean ± SEM is shown. Disappearance times and means beyond 150 min after engulfment are grouped above the dashed blue line. Grey bars show standard deviation of the mean in controls. *$p<0.05$,

**p<0.01, ***p<0.001 compared to control embryos using Student's t-test with Bonferroni correction.

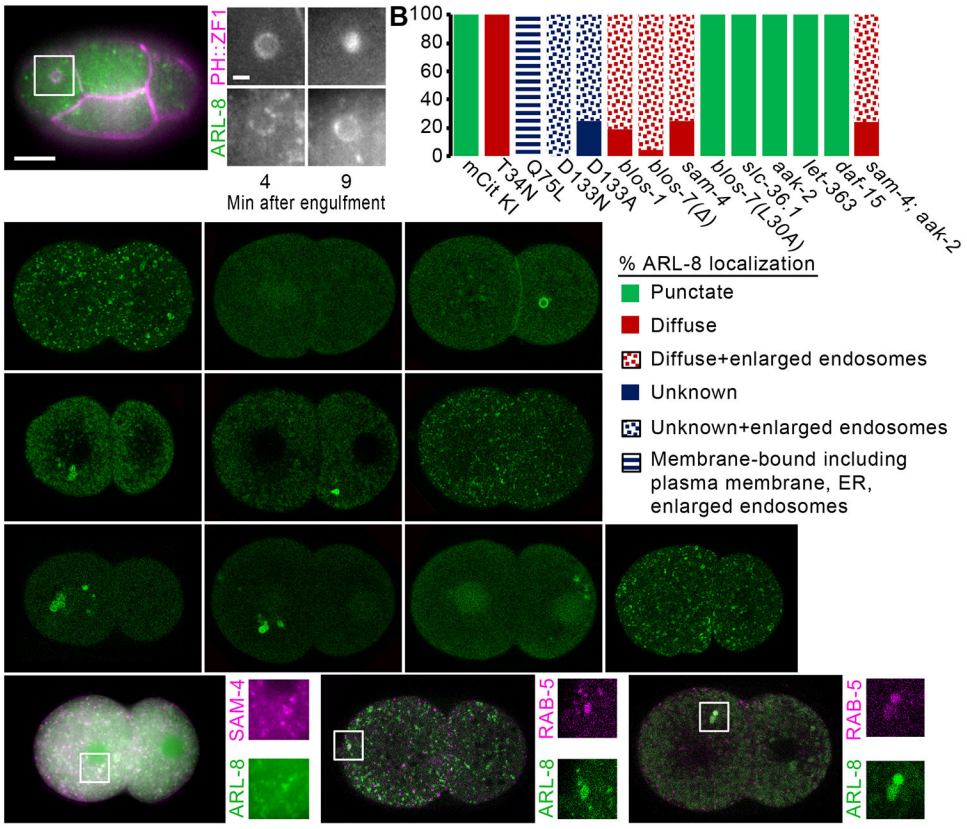

Figure 4: ARL-8 localization to lysosomes, phagolysosomes, and early endosomes depends on GTP cycling

A) ARL-8::mCit puncta (green) appear around the polar body membrane (mCh::PH::ZF1, magenta) shortly after internalization. By the time of the corpse membrane breakdown inside the phagolysosome, ARL-8::mCit appears as a ring around the phagosome. Scale bar is 10 μm. Insets show the magnified dashed white square at the indicated time after engulfment. Scale bar is 2 μm. B) Quantification of ARL-8::mCit localization in ARL-8 or BORC mutants or embryos deficient in TOR-related proteins. See also Figure S4 and S5 for additional mutants and localization to the polar body or phagosome. C) In control embryos, endogenously tagged ARL-8::mCit localizes to puncta (lysosomes and endosomes). D) ARL-8(T34N)::mCit is mostly diffuse. E) ARL-8(Q75L)::mCit localizes to the plasma membrane, ER, and large vesicles. F-G) ARL-8(D133N)::mCit and ARL-8(D133A)::mCit associate with unknown structures in the cytoplasm and large clustered endosomes. H) ARL-8::mCit localizes to puncta after RNAi-mediated *TOR/let*-363 knockdown, similar to control. I-K) In BORC subunit *sam-4(tm3828)*, *blos-1(ok3707)*, or *blos-7(wy1159)* deletion mutants, ARL-8::mCit appears diffuse but also associates with large clustered endosomes. L) ARL-8::mCit localizes to puncta in *blos-7(L30A)* mutants, similar to control. See also Figure S3. M) ARL-8::mCit colocalizes with the lysosomal resident BORC subunit SAM-4. N-O) ARL-8::mCit infrequently colocalizes with the early endosomal marker mCh::RAB-5 (N, Pearson coefficient 0.0003 ± 0.01), while the large clustered endosomes in *arl-8(D133N)* mutants are RAB-5-positive (O).

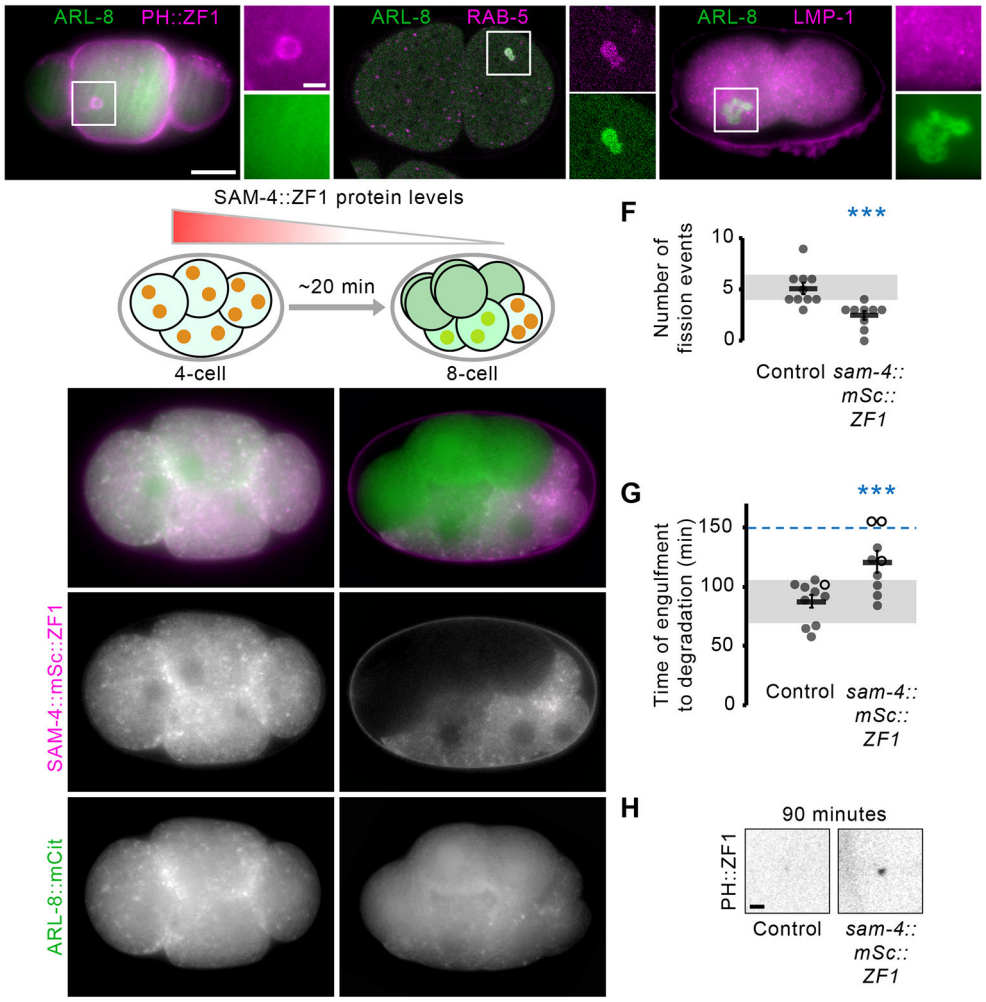

Figure 5: Acute degradation of SAM-4 disrupts ARL-8 localization, phagolysosome tubulation, and resolution

A) ARL-8::mCit (green) does not appear around the polar body membrane (mCh::PH::ZF1, magenta) after engulfment in *sam-4(tm3828)* mutants (see also Figure 4A). B-C) ARL-8::mCit colocalizes with mCh::RAB-5 on large clustered vesicles in *sam-4(tm3828)* mutants (B), but not with lysosomal marker LMP-1 (C). D) SAM-4::mSc::ZF1 (magenta) and ARL-8::mCit (green) colocalize in puncta in a 4-cell embryo prior to the onset of ZIF-1-mediated degradation. E) SAM-4::mSc::ZF1 degrades in the anterior cells of an 8-cell embryo and ARL-8::mCit disperses in the cytosol. In posterior germline cells, ZF1-tagged proteins are not degraded and the punctate pattern of SAM-4 and ARL-8::mCit and their colocalization is conserved. See also Figure S5H for lack of ARL-8::mCit on the phagolysosome after SAM-4::mSc::ZF1 degradation and Figure S6 for lysosome morphology in SAM-4::mSc::ZF1 strain. F) Degrading SAM-4::mSc::ZF1 significantly decreased phagolysosome fission events (2±0 vs. 5±1 in control). G) Disappearance of the 2nd polar body phagolysosome cargo marker mCh::PH::ZF1 was delayed (121±9), compared to control (88±6 min). Open circles denote the last frame of a time-lapse series in which the polar body phagolysosome did not disappear. Mean ± SEM is shown. Disappearance times beyond 150 min after engulfment are grouped above the dashed blue line. Grey bars show

standard deviation of the mean in controls. ***p<0.001 compared to control embryos using Student's t-test. H) Inverted images of corpse phagolysosomes 90 minutes after engulfment in control and a SAM-4::mSc::ZF1 knock-in embryo. Scale bar is 2 μm.

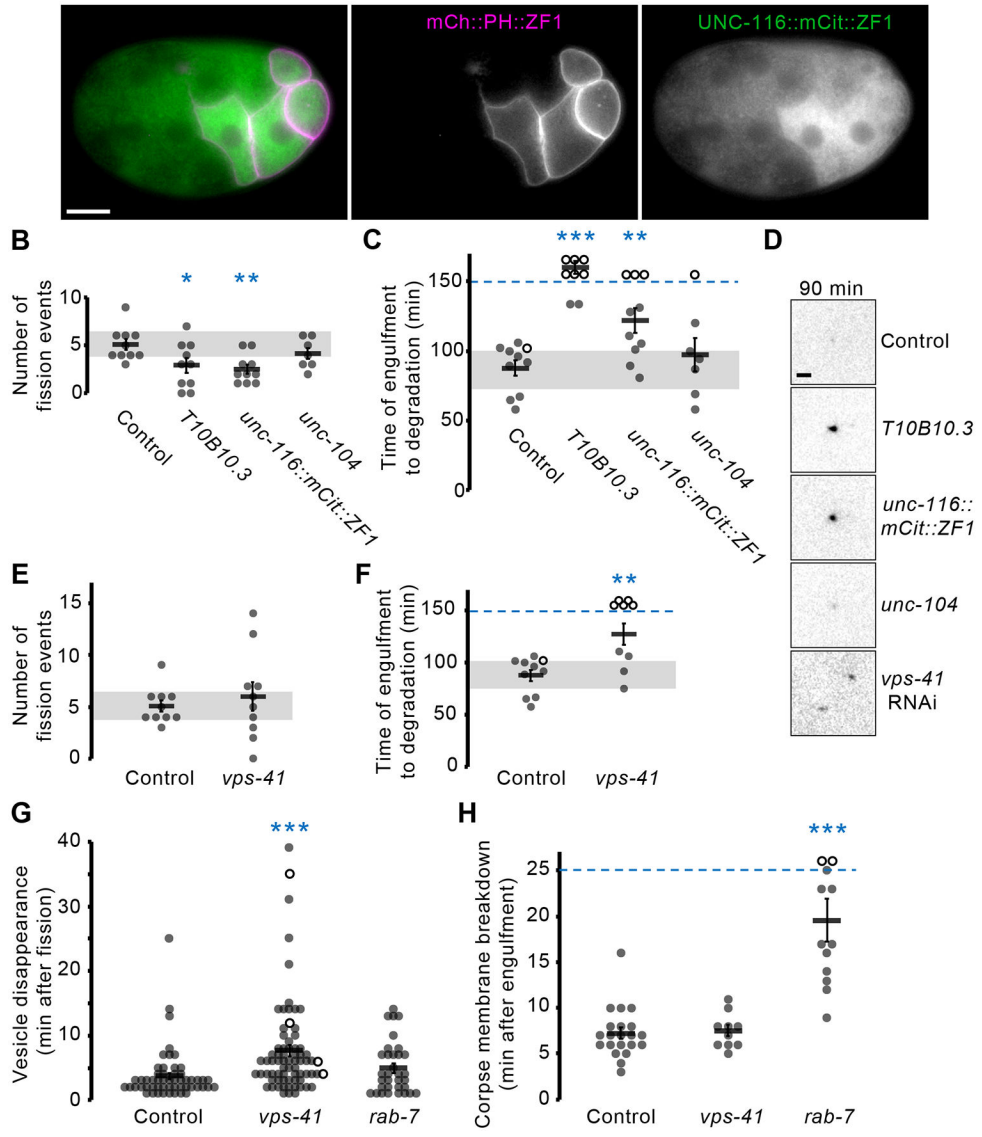

Figure 6: Kinesin-1 drives phagolysosome vesiculation, while HOPS promotes degradation of small phagolysosomal vesicles

A) The KLC5 ortholog UNC-116::mCit::ZF1 (green) degrades in the anterior cells of a 16-cell embryo. mCh::PH::ZF1 (magenta) marks the membrane of posterior cells of the embryo, where UNC-116::mCit::ZF1 is not degraded. Scale bar is 10 μm. B) Phagolysosomal fission events were reduced in *T10B10.3(ok2184)* mutants (3±0) compared to control embryos (5±1). Degrading UNC-116::mCit::ZF1 significantly decreased phagolysosome fission events (3±0), whereas KLC1 mutants *unc-104(e1265)* did not differ from controls (4±1). See also Table S1. C) Disappearance of the 2nd polar body phagolysosome cargo marker mCh::PH::ZF1 was delayed in *T10B10.3(ok2184)* mutants (>150 min) and UNC-116::mCit::ZF1(122±9 min), but not in *unc-104(e1265)* (97±12 min), compared to control (88±6 min). Open circles denote the last frame of a time-lapse series in which the polar body phagolysosome did not disappear. Mean ± SEM is shown. Disappearance times beyond 150 min after engulfment are grouped above the dashed

blue line. Grey bars show standard deviation of the mean in controls. *p<0.05, **p<0.01, ***p<0.001 compared to control embryos using Student's t-test with Bonferroni correction. See also Figure S7 for other PLEKHM family proteins in *C. elegans*. D) Inverted images of corpse phagolysosomes 90 minutes after engulfment in control and embryos of the indicated mutants. Scale bar is 2 μm. E) The number of phagolysosomal fission events was not affected after *vps-41* RNAi (6±1) compared to control embryos (5±1). F) Treatment with *vps-41* RNAi significantly delayed phagolysosome cargo degradation (127±11 min) compared to controls (88±6 min). G) Phagolysosomal vesicles disappear quickly in control embryos (4±1 min) after fission from the phagolysosome, but last twice as long after knockdown of the HOPS subunit *vps-41* (8±1 min). Small vesicles disappear with normal timing after *rab-7* RNAi (5±1 min). Open circles denote the last frame of a time-lapse series in which the vesicle did not disappear. H) Breakdown of the polar body corpse membrane inside the nascent phagolysosome takes 7±1 min in controls. Corpse membrane breakdown is delayed after *rab*-7 knockdown (20±2 min)[4], but not affected after *vps*-41 knockdown (8±1 min).

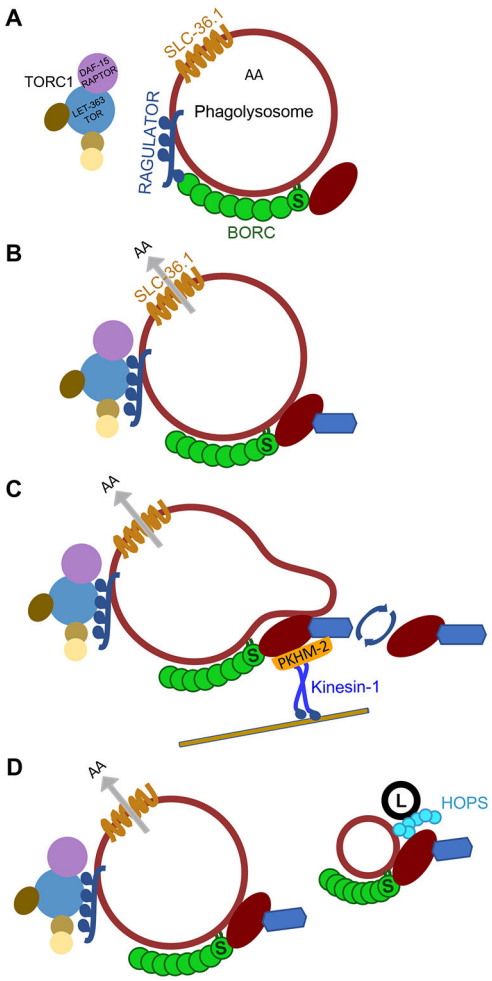

Figure 7: Model of phagolysosome vesiculation

A) After phagosome-lysosome fusion, phagolysosomes are decorated with lysosomal membrane proteins, including solute carriers, Ragulator, and BORC. The BORC subunit SAM-4 (S) recruits nucleotide-free ARL-8 to the phagolysosome membrane. Digestion of corpse cargo by lysosomal hydrolases leads to amino acids in the phagolysosome lumen. B) Amino acids are exported by solute carriers, including SLC-36.1, and amino acids or other breakdown products activate TORC1 to release BORC from Ragulator. SAM-4 promotes GTP-binding by ARL-8. C) ARL-8 needs to cycle between a GDP- and GTP-bound state to maintain its localization and promote tubulation via PKHM-2 and kinesin-1. D) Small phagolysosomal vesicles then fuse with lysosomes (L) using the HOPS tethering complex to facilitate rapid cargo degradation and resolution.

Key Resources Table

REAGENT or RESOURCE	SOURCE	IDENTIFIER
Antibodies		
mouse α-LMP-1	Developmental Studies Hybridoma Bank	AB_2161795
chicken α-GFP	Aves	AB_2307313
Anti-sheep red blood cells rabbit IgG fraction	MP Biomedical	0855806
Bacterial and virus strains		
E. coli B strain, Uracil auxotroph	CGC	OP50
E. coli HT115 expressing empty vector L4440 dsRNA	Source BioScience	*vec* RNAi
E. coli HT115 expressing *daf-15* dsRNA	[51]	*daf-15* RNAi
E. coli HT115 expressing *rict-1* dsRNA	[51]	*rict-1* RNAi
E. coli HT115 expressing *let-363* dsRNA	Source BioScience	*sjj2_B0261.2a*
E. coli HT115 expressing *rub-7* dsRNA	Source BioScience	*mv_E03C9.3*
E. coli HT115 expressing slc-36.1 dsRNA	Source BioScience	*sjj_Y43F4B.7*
E. coli HT115 expressing *vps-41* dsRNA	Source BioScience	*sjj2_F32A6.3*
Biological samples		
Sheep red blood cells	MP Biomedical	0855876
Chemicals, peptides, and recombinant proteins		
MboII	New England Biolabs	R0148S
NlaIV	New England Biolabs	R0126S
Hpy188I	New England Biolabs	R0617S
BstXI	New England Biolabs	R0113S
SalI	New England Biolabs	R0138S
HindIII	ThermoFisher Scientific	ER0501
BclI	New England Biolabs	R0160S
PstI-HF	New England Biolabs	R3140S
Critical commercial assays		
Deposited data		
Experimental models: Cell lines		
Murine macrophage J774 cell line expressing Cas9	[52]	Cas9-expressing J774
Experimental models: Organisms/strains		
lmtr-2(tm2367) V	NBRP	FX2367

REAGENT or RESOURCE	SOURCE	IDENTIFIER
sam-4(tm3828) II	NBRP	FX3828
glo-2(zu455) I; him-5(e1490) V	[53]	GH1077
kxd-1(js1356) I; jsIs973[mec-7p::mRFP; unc-119(+)] III; jsIs821[mec-7p::GFP-RAB-3 unc-119(+)] blos-8(js1354) X	Gift of Michael Nonet	NM4761
blos-9(js1352) I; jsIs973[mec-7p::mRFP; unc-119(+)] III; blos-2(js1351) IV; jsIs821[mec-7p::GFP-RAB-3 unc-119(+)] X	Gift of Michael Nonet	NM4768
Wild type	[54]	N2
cup-14(cd32) II; arIs37[Pmyo-3::ssGFP; dpy-20(+)]	[39]	NP1378
unc-119(ed3) III; ltIs79[pAA196; pie-1::mCherry::RAB-5; unc-119(+)].	[55]	OD179
unc-119(ed3) III; ltIs76[pAA178; pie-1::mCherry::SP12; unc-119(+)]	[56]	OD301
arl-8(jpn1[D133N]) IV	[18]	OTL1
arl-8(wy271) IV; wyIs92[Pmig-13::snb-1::yfp]	[13]	OTL125
arl-8(syb2255[Q75L]) IV	SunyBiotech	PHX2255
arl-8(syb2260[T34N]) IV	SunyBiotech	PHX2260
arl-8(syb2427[arl-8::mCitrine]) IV	SunyBiotech	PHX2427
arl-8(syb2427[arl-8::mCitrine] syb2959[Q75L]) IV	SunyBiotech	PHX2959
arl-8(syb2427[arl-8::mCitrine] syb2960[D133N]) IV	SunyBiotech	PHX2960
arl-8(syb2427[arl-8::mCitrine] syb3085[T34N]) IV / nT1[qIs51] (IV; V)	SunyBiotech	PHX3086
arl-8(syb2427[arl-8::mCitrine] syb3658[D133A]) IV	SunyBiotech	PHX3658
sam-4(syb4007[sam-4::mScarlet-I] II	SunyBiotech	PHX4004
sam-4(syb4105[sam-4::mScarlet-I::ZF1] II	SunyBiotech	PHX4105
unc-116(syb5797[unc-116::mCit::ZF1] III	SunyBiotech	PHX5797
ctns-1(syb5851[ctns-1::mCitrine]) II	SunyBiotech	PHX5851
blos-7(syb6675[L30A]) IV	SunyBiotech	PHX6675
aak-2(ok524) X	CGC	RB754
unc-104(e1265) II	[18]	TV459
blos-7(wy1159) IV; wyIs546[Podr-1::gfp, Pitr-1::arl-8::yfp, Pitr-1::mCh::rab-3]	[18]	TV22791
T10B10.3(ok2184) X	CGC	VC1682
blos-1(ok3707) III	CGC	VC3015
unc-119(ed3) III; pwIs20[pie-1::gfp::rab-5; unc-119(+)]; mCherry::HistoneH2B IV	[4]	WEH246
wurIs90[pGF7: pie-1::mCherry::PH(PLC1∂1)::ZF1, unc-119(+)] II; unc-119(ed3) III	[57]	WEH260
unc-119(ed3) III; wurIs92[pGF7:pie-1::mCh::PH::ZF1, unc-119(+)]	Bombardment	WEH262
cup-14(cd32) II; unc-119(ed3) III; wurIs90[pGF7:pie-1::mCh::PH::ZF1, unc-119(+)] C2	Crossed WEH260 x NP1378	WEH340
wurIs118[lmp-1::TY1::GFP::FLAG fosmid, unc-119(+)] I; unc-119(ed3) III	Bombardment	WEH350
wurIs90[pGF7:pie-1::mCh::PH::ZF1, unc-119(+)] II; unc-119(ed3) III; aak-2(ok524) X	Crossed WEH260 x RB754	WEH436
wurIs118[lmp-1::TY1::GFP::FLAG fosmid, unc-119(+)]I; wurIs90[pGF7:pie-1::mCh::PH::ZF1, unc-119(+)] II; unc-119(ed3) III	Crossed WEH260 x WEH350	WEH494

REAGENT or RESOURCE	SOURCE	IDENTIFIER
wurIs90[pGF7:pie-1::mCh::PH::ZF1, unc-119(+)]III; unc-119(ed3) III; blos-7(wy1159) IV	Crossed WEH260 x TV22791	WEH495
sam-4(tm3828) wurIs90[pGF7:pie-1::mCh::PH::ZF1, unc-119(+)] II; unc-119(ed3) III	Crossed WEH260 x FX3828	WEH496
wurIs90[pGF7:pie-1::mCh::PH::ZF1, unc-119(+)] II; unc-119(ed3) III; arl-8(jpn1[D133N]) IV	Crossed WEH260 x OTL1	WEH503
wurIs90[pGF7:pie-1::mCh::PH::ZF1, unc-119(+)] II; blos-1(ok3707), unc-119(ed3) III	Crossed WEH260 x VC3015	WEH504
unc-104(e1265) II; unc-119(ed3) III; wurIs92[pGF7:pie-1::mCh::PH::ZF1, unc-119(+)]	Crossed WEH262 x TV459	WEH517
wurIs90[pGF7:pie-1::mCh::PH::ZF1, unc-119(+)] II; unc-119(ed3) III; arl-8(syb2260[T34N]) IV	Crossed WEH260 x PHX2260	WEH533
wurIs90[pGF7:pie-1::mCh::PH::ZF1, unc-119(+)] II; unc-119(ed3) III; arl-8(syb2255[Q75L]) IV	Crossed WEH260 x PHX2255	WEH536
glo-2(zu455) I; wurIs90[pGF7:pie-1::mCh::PH::ZF1, unc-119(+)] II; unc-119(ed3) III	Crossed WEH260 x GH1077	WEH557
wurIs90[pGF7:pie-1::mCh::PH::ZF1, unc-119(+)] II; unc-119(ed3) III; arl-8(syb2427[arl-8::mCitrine]) IV	Crossed WEH260 x PHX2427	WEH558
blos-9(js1352) I; wurIs90[pGF7:pie-1::mCh::PH::ZF1, unc-119(+)] II; unc-119(ed3) III	Crossed WEH260 x NM4768	WEH564
wurIs90[pGF7:pie-1::mCh::PH::ZF1, unc-119(+)] II; unc-119(ed3) III, blos-2(js1351) IV	Crossed WEH260 x NM4768	WEH566
sam-4(tm3828) wurIs90[pGF7:pie-1::mCh::PH::ZF1, unc-119(+)] II; unc-119(ed3) III; arl-8(syb2427[arl-8::mCitrine]) IV	Crossed WEH558 x WEH496	WEH570
kxd-1(js1356) I; wurIs90[pGF7:pie-1::mCh::PH::ZF1, unc-119(+)] II, unc-119(ed3) III; blos-8(js1354) X	Crossed WEH260 x NM4761	WEH575
wurIs90[pGF7:pie-1::mCh::PH::ZF1, unc-119(+)] II, unc-119(ed3) III; blos-8(js1354) X	Crossed WEH260 x WEH575	WEH579
kxd-1(js1356) I; wurIs90[pGF7:pie-1::mCh::PH::ZF1, unc-119(+)] II, unc-119(ed3) III	Crossed WEH260 x WEH575	WEH580
wurIs90[pGF7:pie-1::mCh::PH::ZF1, unc-119(+)] II, unc-119(ed3) III; arl-8(syb2427[arl-8::mCitrine] syb2959[Q75L]) IV	Crossed WEH260 x PHX2959	WEH597
wurIs90[pGF7:pie-1::mCh::PH::ZF1, unc-119(+)] II, unc-119(ed3) III; arl-8(syb2427[arl-8::mCitrine] syb2960[D133N]) IV	Crossed WEH260 x PHX2960	WEH600
unc-119(ed3) III; arl-8(syb2427[arl-8::mCitrine] syb2960[D133N]) IV; ltIs79[pAA196: pie-1::mCherry::RAB-5; unc-119(+)].	Crossed PHX2960 x OD179	WEH602
wurIs90[pGF7:pie-1::mCh::PH::ZF1, unc-119(+)] II, unc-119(ed3) III; arl-8(syb2427[arl-8::mCitrine] syb3085[T34N]) IV / nT1[qIs51] (IV; V)	Crossed WEH260 x PHX3086	WEH604
wurIs90[pGF7:pie-1::mCh::PH::ZF1, unc-119(+)] II, unc-119(ed3) III; arl-8(wy271) IV	Crossed WEH260 x OTL125	WEH612
arl-8(syb2427[arl-8::mCitrine]) IV; ltIs79[pAA196: pie-1::mCherry::RAB-5, unc-119(+)]	Crossed OD179 x WEH570	WEH616
wurIs90[pGF7:pie-1::mCh::PH::ZF1, unc-119(+)] II; unc-119(ed3) III; arl-8(syb2427[arl-8::mCitrine]) IV; aak-2(ok524) X	Crossed WEH436 x WEH570	WEH625
sam-4(tm3828) wurIs90[pGF7:pie-1::mCh::PH::ZF1, unc-119(+)] II; unc-119(ed3) III; arl-8(syb2427[arl-8::mCitrine]) IV; aak-2(ok524) X	Crossed WEH436 x WEH570	WEH626
sam-4(tm3828) wurIs90[pGF7:pie-1::mCh::PH::ZF1, unc-119(+)] II; unc-119(ed3) III; aak-2(ok524) X	Crossed WEH436 x WEH570	WEH627
wurIs90[pGF7:pie-1::mCh::PH::ZF1, unc-119(+)] II; blos-1(ok3707), unc-119(ed3) III; arl-8(syb2427[arl-8::mCitrine]) IV	Crossed WEH558 x WEH504	WEH629

REAGENT or RESOURCE	SOURCE	IDENTIFIER
wurIs90[pGF7:pie-1::mCh::PH::ZF1, unc-119(+)] II, unc-119(ed3) III; arl-8(syb2427[arl-8::mCitrine] syb3658[D133A]) IV	Crossed WEH260 x PHX3658	WEH630
wurIs90[pGF7:pie-1::mCh::PH::ZF1, unc-119(+)] II, unc-119(ed3) III; arl-8(syb2427[arl-8::mCitrine] blos-7(wy1159) IV	Crossed WEH558 x WEH495	WEH631
wurIs90[pGF7:pie-1::mCh::PH::ZF1, unc-119(+)] II; unc-119(ed3) III; arl-8(wy271) IV; aak-2(ok524) X	Crossed WEH436 x WEH612	WEH636
arl-8(syb2427[arl-8::mCitrine] syb3658[D133A]) IV; ltIs76[pAA178; pie-1::mCherry::SP12; unc-119 (+)]	Crossed OD301 x PHX3658	WEH638
sam-4(syb4007[sam-4::mScarlet-I] II; arl-8(syb2427[arl-8::mCitrine]) IV	Crossed WEH558 x PHX4007	WEH640,WEH641
sam-4(syb4105[sam-4::mScarlet-I::ZF1] II; arl-8(syb2427[arl-8::mCitrine]) IV	Crossed WEH558 x PHX4105	WEH644
wurIs90[pGF7:pie-1::mCh::PH::ZF1, unc-119(+)] II; unc-119(ed3) III; arl-8(syb2427[arl-8::mCitrine]) IV; lmtr-2(tm2367) V	Crossed WEH260 x FX2367	WEH645
arl-8(syb2427[arl-8::mCitrine] syb2959[Q75L]) IV; ltIs76[pAA178; pie-1::mCherry::SP12; unc-119(+)]	Crossed WEH597 x OD301	WEH646
wurIs90[pGF7:pie-1::mCh::PH::ZF1, unc-119(+)] II; unc-119(ed3) III; lmtr-2(tm2367) V	Crossed WEH260 x FX2367	WEH649
sam-4(syb4105[sam-4::mScarlet-I::ZF1]) wurIs90[pGF7:pie-1::mCh::PH::ZF1, unc-119(+)] II; arl-8(syb2427[arl-8::mCitrine]) IV	Crossed WEH558 x PHX4105	WEH650
sam-4(tm3828) II, arl-8(syb2427[arl-8::mCitrine]) IV; ltIs79[pAA196; pie-1::mCherry::RAB-5; unc-119(+)]	Crossed OD179 x FX3828	WEH663
sam-4(syb4105[sam-4::mScarlet-I::ZF1] wurIs90[pGF7:pie-1::mCh::PH::ZF1, unc-119(+)] II	Crossed N2 x WEH650	WEH666
sam-4(syb4007[sam-4::mScarlet-I]) II; unc-119(ed3) III; pwIs20[pie-1::gfp::rab-5; unc-119(+)]	Crossed WEH641 x WEH246	WEH686
wurIs90[pGF7:pie-1::mCh::PH::ZF1, unc-119(+)] II; unc-116(syb5797[unc-116::mCit::ZF1] III	Crossed WEH260 x PHX5797	WEH688
sam-4(syb4007[sam-4::mScarlet-I]) ctns-1(syb5851[ctns-1::mCitrine]) II; unc-119(ed3) III	Crossed WEH686 x PHX5851	WEH690
sam-4(syb4105[sam-4::mScarlet-I::ZF1]) ctns-1(syb5851[ctns-1::mCitrine]) II	Crossed PHX5851 x PHX4105	WEH699
wurIs90[pGF7:pie-1::mCh::PH::ZF1, unc-119(+)] II; unc-119(ed3) III; T10B10.3(ok2184) X	Crossed VC1682 x WEH260	WEH702
wurIs90[pGF7:pie-1::mCh::PH::ZF1, unc-119(+)] II, unc-119(ed3) III; blos-7(syb6675[L30A]) IV	Crossed WEH260 x PHX6675	WEH704
wurIs90[pGF7:pie-1::mCh::PH::ZF1, unc-119(+)] II, unc-119(ed3) III; blos-7(syb6675[L30A]) arl-8(syb2427[arl-8::mCitrine] IV	Crossed PHX6675 x WEH558	WEH705
Oligonucleotides		
CTTCAGCTCGTCTCAATGTACCT	This study	cup-14 exon 11 F
GACTACAGTACTCAAGGCTACAGT	This study	cup-14 intron 11 R
CTG AAA CAG AAA GCG CTG GTT G	This study	lmtr-2_ex1_F
GGA TGG GAT GAA TGA GAC CCG	This study	lmtr-2_3'UTR_R
GCT CAT CAA GTG CTC CAG GAA C	This study	arl-8_D133A_NlaVI_R
CAACAAGAACGACTACCTGGC	This study	kxd-1_ex1_F
CGTCGATTTGAGAAGTGAGCG	This study	kxd-1_ex2_R
AAG AAG ACG GAT AAA TTC CCC G	Gift of Michael Nonet	oMN_5501(blos-9_F)

REAGENT or RESOURCE	SOURCE	IDENTIFIER
CCT TGA AGT CTG TAC AGC GC	Gift of Michael Nonet	oMN_5502(blos-9_R)
GTC TAA AGA TGC ACC ATC GTT ACA C	Gift of Michael Nonet	oMN_5503(blos-8_F)
CAC CCT TTT TCC ATA TCC TCA GC	Gift of Michael Nonet	oMN_5504(blos-8_R)
CGT GTC GAG ACC TGG TGC CG	Gift of Michael Nonet	oMN_5509(blos-2_F)
GCA AAA GGG AGG GAG CAA AAT TAG C	Gift of Michael Nonet	oMN_5517b(blos-2_R)
CCA GTT TTC CAG CCA CCT TCT CC	Gift of Michael Nonet	oMN_5518(blos-2_Mid)
TCA CTG GAT GTC GTT GGA AA	This study	aak-2 ok524 F
AGT AGT CAA CGC CGG AAA TG	This study	aak-2 ok524 inner R
ATC ATC AAA TGG CAG GGT TC	This study	aak-2 ok524 R
CGCTGCTTGCCCACCGAATACATAA	This study	blos-7_wy1159_1
CATGTCCAATGTGCTACGCGAG TTTC	This study	blos-7_wy1159_2
CAAATCGTCGACTACGAAGGACGTCTG	This study	blos-7_wy1159_3
TCG CTT CAA CAC TCT TGC AA	This study	oGF024(sam-4_F)
GCG GGC ACA TCA TCT AAT CC	This study	oGF025(sam-4_R)
CGA TGT GGG AAC GAT ATT GCC	This study	oGF029(arl-8_jpn1_F)
ATG GAG GGG AGG GGA TTC	This study	oGF030(arl-8_jpn1_R)
CGG ATT CAA TAT GCG GAA GA	This study	oGF031(arl-8_Q75L_F)
GAGCACCAAAACTGGAATAG	This study	oGF032(arl-8_Q75L_R)
CTG TGT CCG CTT GAG AAA TTT G	This study	oGF033(arl-8_T34N_F)
GGTTTGAGCTGCCACGATA	This study	blos-1 exon 2 R1
GAA GCT CAG TTG AGG GTT G	This study	ok3707_ext_R
TTG TGA AGG AGA TTG CAA CG	This study	ok3707_ext_F
CCT CGT CCC TCG TGA GGA AAA AGT TGC	This study	blos-7_5UTR_F
CGT GCA CTT TCA CGG ATC CGT TCG TC	This study	blos-7_Ex1_R
CCGCACAACATATGACGAATTGT	This study	T10B10.3 prom F1
GGATTCTTGCGCCTTCTCAAC	This study	T10B10.3 exon 8 F3
TCATCATCAAGCTTTGCCCAAC	This study	T10B10.3 exon 8 R
GAAATGGATCTAACGCAGC	This study	sgRNA Control
GATGGACGATATCGTGG	This study	sgRNA Myrlysin
GACCGAAAGCTCCGGCTC	This study	sgRNA Lyspersin
Recombinant DNA		
pie-1::mCh::PH::ZF1, unc-119(+)	[4]	pGF7

REAGENT or RESOURCE	SOURCE	IDENTIFIER
WRM0636B_G02(pRedFlp-Hgr) (lmp-1[21661]::S0001_pR6K_Amp_2xTY1ce_EGFP_FRT_rpsl_neo_FRT_3x Flag)dFRT::unc-119-Nat	[58]	lmp-1::TY1::GFP::FLAG fosmid, unc-119(+)
Software and algorithms		
Imaris 9.0.2	Oxford Instruments	https://imaris.oxinst.com
Illustrator 26.0.1	Adobe	https://www.adobe.com/de/products/illustrator.html
Photoshop 23.0.2	Adobe	https://www.adobe.com/de/products/photoshop.html
TIDE 3.3.0	The Netherlands Cancer Institute	https://tide.nki.nl
Other		